STRUCTURAL BIOLOGY

DET1 dynamics underlie cooperative ubiquitination by CRL4$^{DET1\text{-}COP1}$ complexes

Abigail E. Burgess[1]†, Tarren A. Loughran[1]†, Liam S. Turk[1], Hunter G. Nyvall[2], Jessica L. Dunlop[1], Sam A. Jamieson[1], Jack R. Curry[1], John E. Burke[2,3], Pavel Filipcik[1]‡, Simon H. J. Brown[4], Peter D. Mace[1]*

Transcription factor ubiquitination is a decisive regulator of growth and development. The DET1-DDB1-DDA1 (DDD) complex associates with the Cullin-4 ubiquitin ligase (CRL4) and a second ubiquitin ligase, COP1, to control ubiquitination of transcription factors involved in neurological, metabolic, and immune cell development. Here, we report the structure of the human DDD complex, revealing a specific segment of DET1 that can recruit ubiquitin-conjugating (E2) enzymes. Structural variability analysis, mass spectrometry, and mutagenesis based on AlphaFold predictions suggest that dynamic closure of DET1, stabilized by DDA1, underlies coordinated recruitment of E2 enzymes and COP1. Biochemical assays suggest that the E2 acts as a recruitment factor to bring COP1 to DET1 for more effective substrate ubiquitination, which parallels a catalytically inactive E2 enzyme (COP10) in plant DDD complexes. This work provides a clear architecture for regulation and cooperative CRL4$^{DET1\text{-}COP1}$ complex assembly, which can affect degradation of diverse targets by COP1 complexes.

INTRODUCTION

Posttranslational modification of proteins with ubiquitin is one of the most pervasive signals in biology. Ubiquitin modifications can range from a single ubiquitin molecule to chains linked at lysine branch points, which mediate a range of fates for modified proteins. Chains linked through ubiquitin lysine-48 or lysine-11 promote degradation of modified proteins by the proteasome (*1*, *2*). One core function of degradative ubiquitination is in regulating levels of transcription factors—attachment of degradative ubiquitin chains to induce proteasomal degradation removes specific transcription factors from the cell and allows remodeling of the prevailing transcriptional program. Transcriptional regulation by ubiquitin is mediated by an array of different ubiquitin ligases, including stand-alone ubiquitin ligases, and multimeric complexes with interchangeable modules to enable regulation of different sets of substrates.

Cullin-4 (CUL4) is a major nuclear platform for building ubiquitin chains (*3*–*5*). Like all Cullin ligases, CUL4 acts as a scaffold via which ubiquitin is transferred via an E3 ligase Really Interesting New Gene (RING) protein, Rbx1 (Fig. 1A) (*6*). Within CUL4 complexes, the RING domain of Rbx1 binds to a ubiquitin-conjugating (E2) enzyme, and a ubiquitin molecule loaded from that E2 is transferred to targets recruited by substrate adapters. Substrate adapters for CUL4 are recruited through the DNA damage binding protein 1 (DDB1), which both binds the N-terminal region of CUL4 and recruits one of the many DDB1 and CUL4-associated factors (DCAFs) (*7*). Regulation of the CUL4 complex and related Cullin complexes' activity comes at several levels, including modification by the ubiquitin-like molecule NEDD8 and exchange of DCAF proteins (*8*–*10*). DCAF proteins are key to the specificity of CUL4-substrate complexes (*7*), and individual DCAF proteins have received considerable attention as recruitment modules in the field of targeted protein degradation (*11*).

Among DCAFs, De-etiolated-1 (DET1) is a highly conserved module retained from plants to humans, with DET1 in plants being a crucial mediator of light-regulated development (*12*–*14*). There is some suggestion of DET1 regulation by light in animals (*15*), but it is unclear whether light is the main determinant of substrate degradation. In both plants and humans, DET1 forms a complex with DDB1 and DDA1, which overall is known as the DDD complex. The DDD complex can exist in isolation or be incorporated into CUL4 complexes, where it is assumed to act as a substrate recruitment module (*16*). That said, the DDD complex has also been suggested to directly impede CUL4-based ubiquitination (*16*). DET1 is also somewhat unique among DCAF proteins in that it can directly bind (E2) ubiquitin-conjugating enzymes, specifically the human Ube2e family, through an ill-defined mechanism (*16*). The exact role played by recruited E2s within the DDD complex is currently unclear, and there have been few direct substrates reported to directly bind human DET1.

Despite a lack of direct substrates being identified, human DET1 is known to recruit another ubiquitin ligase, Constitutive Photomorphogenic 1 (COP1) into complexes with CUL4 (CRL4$^{DET1\text{-}COP1}$) (*17*, *18*). Like DET1, COP1 was first identified in plants as a major regulator of light-mediated development through transcription factor degradation (*13*). Analogously, human COP1 regulates ubiquitination of a range of key developmental transcription factors including p53, c-Jun, and ETS and C/EBP families (*14*, *18*–*21*). Through this activity, COP1 has been shown to regulate immune, glial, hepatic, and pancreatic cells and be relevant to traditional cancer treatments based on kinase inhibition and immune checkpoint blockade therapy (*22*–*27*).

COP1 contains an N-terminal RING domain, a central coiled-coil region, and a C-terminal WD40 domain primarily responsible for substrate recruitment. Although these domains give capacity to both recruit substrates and promote ubiquitin transfer, COP1 appears to have

[1]Department of Biochemistry, School of Biomedical Sciences, University of Otago, Dunedin, New Zealand. [2]Department of Biochemistry and Microbiology, University of Victoria, Victoria, BC, Canada. [3]Department of Biochemistry and Molecular Biology, University of British Columbia, Vancouver, BC, Canada. [4]School of Chemistry and Molecular Bioscience, Molecular Horizons, and Australian Research Council Centre for Cryo-electron Microscopy of Membrane Proteins, University of Wollongong, Wollongong, NSW, Australia.
*Corresponding author. Email: peter.mace@otago.ac.nz
†These authors contributed equally to this work.
‡Present address: Paul Scherrer Institute, Villigen, Switzerland.

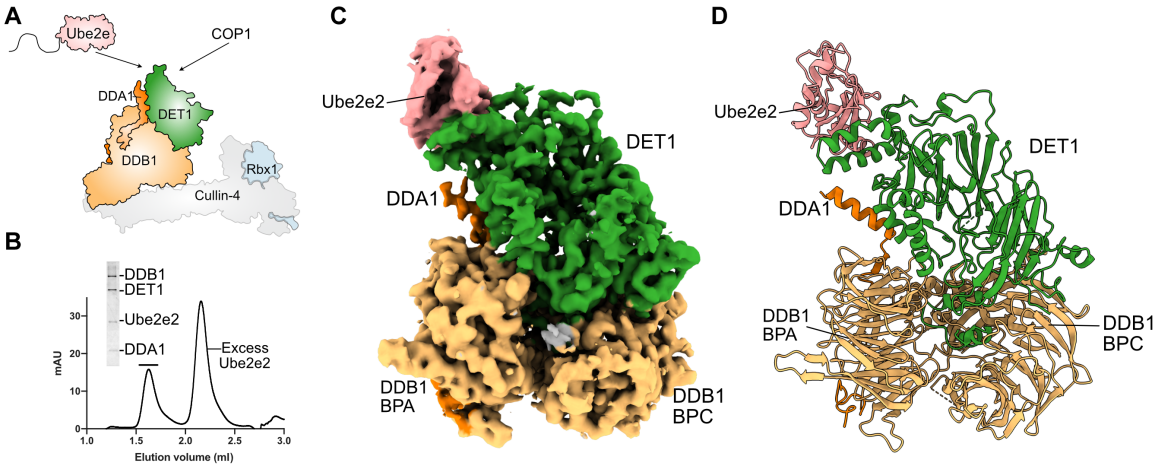

Fig. 1. Structure of the DDD-Ube2e2 complex. (**A**) Schematic representation of the DDD complex. (**B**) Purification of Ube2e2 with the DDD complex. DDD complex was purified using size exclusion with an excess of Ube2e2. mAU, milli absorbance units. (**C**) Cryo-EM density of the DDB1(ΔBPB)-DET1-DDA1-Ube2e2 complex. (**D**) Molecular model of the DDB1(ΔBPB)-DET1-DDA1-Ube2e2 complex. DET1 (green), DDB1(ΔBPB) (yellow), DDA1 (orange), and Ube2e2 (pink).

multiple modes of activity—ubiquitinating some substrates bound to its WD40 domain with its own RING domain and other substrates independently of its RING domain when COP1 associates with specific $CRL4^{DET1}$ complexes. Binding between COP1 and DET1 is known to be regulated by extracellular signal–regulated kinase (ERK) family mitogen-activated protein (MAP) kinase phosphorylation (*21*), and mutations in either *DET1* or *COP1* in cancer can drive resistance to ERK pathway–targeted therapies (*27*).

Complexes formed by DET1 and COP1 clearly play a key role in the developmental programming within normal cells, disease progression, and therapeutic resistance. However, the architecture of complexes that contain both CRL4 and DET1, with or without COP1 is currently unclear, and the roles of two different ubiquitin ligase activities (COP1 and Rbx1) in the complex is currently unclear. Why DET1 retains the ability to bind to E2 enzymes and why that binding is specific for the Ube2e family remain to be determined. Here, we use a combination of cryo–electron microscopy (cryo-EM), site-directed mutagenesis, hydrogen-deuterium exchange mass spectrometry (HDX-MS), binding studies, and AlphaFold modeling to demonstrate that DET1 forms a dynamic recruitment module that specifically recruits Ube2e family E2s. Stabilization of DET1 by the DDA1 protein is required for COP1 binding adjacent to the Ube2e binding site. Overall, multifaceted interactions combine to stabilize inherently dynamic constituents and allow assembly of the intact $CRL4^{DET1\text{-}COP1}$ complex.

RESULTS

Architecture of the human DDD-Ube2e2 complex

To gain insight into the interactions and function of the DDD complex, we established a system to coexpress and purify the human DDD complex with full-length Ube2e2. Following affinity purification, subsequent purification by size exclusion chromatography showed that a considerable proportion of Ube2e2 was retained in a high–molecular weight complex with core DDD components (Fig. 1B). Full-length DDB1, DET1, DDA1, and Ube2e2 were used for initial structure determination by cryo-EM, which resolved all four components but showed severe map anisotropy indicative of particle orientation bias (fig. S1). We subsequently purified the DDD complex using DDB1 where the central WD40 domain of DDB1 [BPB (*28*)] was deleted. The BPB domain normally mediates CUL4 binding but can exhibit considerable flexibility (*29*) and has been deleted to facilitate high-resolution structures of other DCAF proteins (*30*, *31*). Eventual maps of DDD(ΔBPB)-Ube2e2 markedly improved map quality and allowed modeling of continuous density for most of the complex to a Fourier shell correlation (FSC)–determined resolution of 2.84 Å (Fig. 1C, Table 1, and fig. S2).

The overall model of the DDD(ΔBPB)-Ube2e2 complex (Fig. 1D) shows the N-terminal H-box motif of DET1 interacting with the BPC of DDB1, similar to other comparable DCAF-DDB1 structures but with some subtle differences (fig. S3) (*7*). The arrangement of DET1 in the BPC pocket is most similar to DCAF1 and DCAF15, binding via a helix-loop-helix motif. This mode of interaction is relatively minimal compared to interactions of Cereblon, DDB2, and DCAF16, which each contain additional elements mediating interactions with DDB1 (fig. S3).

Beyond the N-terminal region, DET1 is composed of a predominantly β sheet structure, which overlays relatively well with the AlphaFold2 predicted structure of DET1 [root mean square deviation (RMSD) of pruned atom pairs: 0.931 Å, across all 508 atom pairs: 1.288 Å; fig. S4]. The major departure of DET1 from its β sheet core is an insertion of residues 262 to 329, which form a series of α helices propagating from the core at approximately right angles. This has the effect of forming a "cup" within which the core ubiquitin-conjugating domain of Ube2e2 is well defined by cryo-EM density (Fig. 1C). The extended structure of DDA1 wraps around DDB1—with residues 3 to 17 binding to the bottom of the BPA WD40 domain and its C-terminal helix (residues 54 to 68) interacting below the E2 binding site of DET1 (Fig. 1C and fig. S4B). The segment connecting residues 17 to 42 of DDA1 is largely undefined by cryo-EM density.

Dynamic nature of DET1

A range of subclasses that were identified during three-dimensional (3D) classification suggested that DDD complexes have variable degrees of order (Fig. 2). 3D variability analysis and clustering revealed that only a subset of particles that contained DET1 and DDB1 had a

Table 1. Cryo-EM data collection, refinement, and validation statistics.

Data collection and processing	DDD(ΔBPB) complex	Cluster 2
Magnification	×130,000	×130,000
Voltage (keV)	300	300
Electron exposure (e^{-}/Å^2)	80	80
Defocus (μm)	−1.0	−1.0
Pixel size (Å)	0.65	0.65
Symmetry imposed	C1	C1
Final particle images (no.)	61,234	70,496
Map resolution FSC threshold	0.143	0.143
Map resolution (Å)	2.83	3.02
Refinement		
Initial model used (PDB)	AlphaFold	
Model composition		
Nonhydrogen atoms	11,999	
Protein residues	1527	
B factor (Å^2)		
Minimum	70.82	
Maximum	281.24	
Mean	154.54	
RMSDs		
Bond lengths (Å)	0.002	
Bond angles (°)	0.531	
Validation		
MolProbity score	1.63	
Clashscore	7.89	
Rotamer outliers (%)	0.15	
Ramachandran plot		
Favored (%)	96.75	
Allowed (%)	3.25	
Outliers (%)	0	

density corresponding to the full DET1 protein bound to Ube2e2 (Fig. 1C, cluster 1, and fig. S2). Another set of particles had a density corresponding to most of DET1, but the cup of DET1 could not be resolved nor was there any visible density for Ube2e2 (cluster 2; refined to 3.0 Å; Fig. 2). An even larger set of particles (65% of DDB1-DET1 containing particles, clusters 3 to 5) showed relatively clear density for the section of DET1 that sits above the BPC domain of DDB1 (residues 12 to 160 and 449 to 550) but little density for parts of DET1 that sit above the BPA domain. Further evidence for this dynamic behavior was present in the data collected for the DDD complex with full-length DDB1, where data anisotropy prevented detailed model building, but DET1 in general appeared to be in a relatively open state (fig. S1C).

The difference between the densities for DET1 among subclassified particles suggests that these regions of DET1 may be flexible and undergo dynamic unfolding to move between a "closed" state and a more open state. In the structures where DET1 is closed, the C-terminal helix of DDA1 interacts with DET1 (Fig. 2). However, in the more open classes, there is disparate density for DDA1 (Fig. 2, A and B), indicating that DDA1 and DET1 stabilization may be linked. When viewed at equivalent contour levels in the DDB1 region, which is consistently well defined, the more open classes lack density corresponding to either N- or C-terminal portions of DDA1 (Fig. 2B). This suggests that classes where DET1 is most disordered also have low overall DDA1 occupancy.

To further assess whether the flexibility that was observed was a reflection of the flexibility of the complex rather than an artifact of the cryo-EM sample preparation, we used HDX-MS (Fig. 2C). The extent of deuterium incorporation is primarily determined by the stability of protein secondary structure and solvent accessibility with highly dynamic, exposed regions exchanging rapidly (milliseconds to seconds), with stable secondary structure exchanging slowly (minutes to hours) (*32*). To further understand the intrinsic dynamics of the DDD E2 complex, deuterium incorporation was analyzed following a brief pulse of deuterium exposure (3 s at 0°C). Under these conditions, only amides with very little to no secondary structure will be labeled (*33*, *34*). We were able to map deuterium exchange on all four proteins in the DDD E2 complex, with the full coverage statistics and deuterium incorporation information fully available in the source data (Fig. 2, C and D, and data S1).

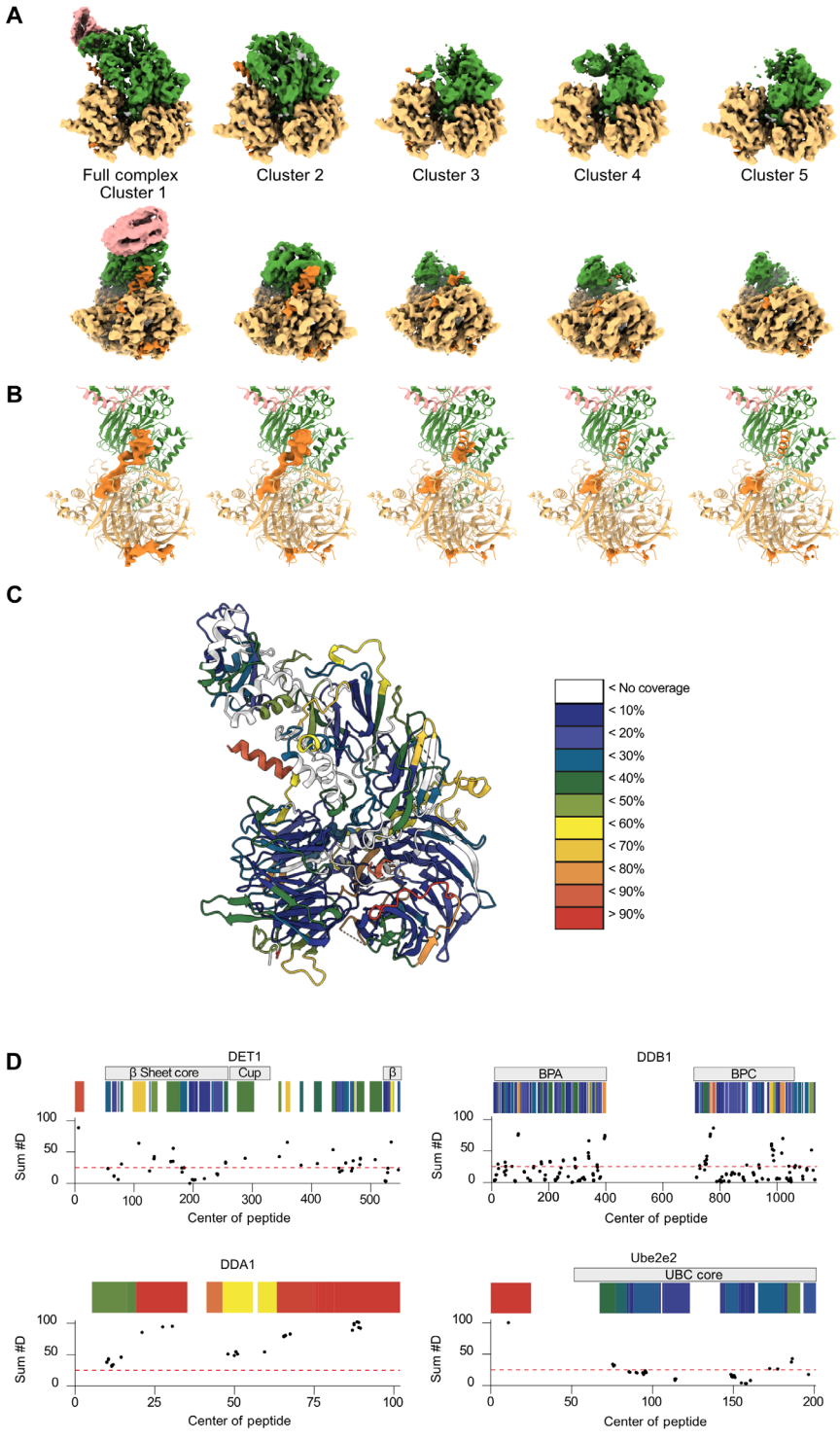

Fig. 2. DET1 and DDA1 are dynamic components of the DDD. (**A**) Structures of DET1 from different clusters (fig. S2B). Complexes with density for all the components of the full DDD(ΔBPB) complex define the closed state. (**B**) DDA1 density across different classes in (A). The full complex and cluster 2, the most complete models displayed, contain more density for DDA1 than clusters 3 to 5, where DDA1 density is disparate, indicating that DDA1 may lock the complex into the closed state. (**C**) HDX-MS analysis of the DDD(ΔBPB)-E2 complex revealed varying degrees of flexibility for different regions of the complex. The regions identified as more flexible by HDX-MS correspond to regions absent in the clusters with sparse density. DDA1 and DET1 contained the most flexibility. (**D**) Percent (%) deuterium incorporation after 3 s at 0°C. Data are absolute deuterium incorporation as back-exchange was normalized using a fully deuterated control. Each point represents a single peptide, which is graphed according to central residue. Heatmap above is color coded according to the legend. Dashed line indicates regions with a % deuterium incorporation above 25%. Full deuterium incorporation for all peptides is available in data S1.

The most stable of the four components was DDB1, with most of the protein showing deuterium incorporation below 25%, highlighting that DDB1 is quite stable. Comparing this to DET1, only the β strand core of DET1 showed deuterium incorporation below 25%, with large regions showing more extensive hydrogen-deuterium exchange. The most dynamic protein was DDA1, with the highest levels of deuterium incorporation, highlighting the dynamic nature of this interfacial DDA1 helix. Overall, this is indicative of DET1, Ube2e2, and DDA1 being more intrinsically flexible relative to the stable DDB1. This aligns with the loss of DET1 density observed in the more disordered classes of the cryo-EM data, whereas the density of DDB1 remained largely constant.

Model of the COP1-DET1 complex

To investigate how DET1 dynamics may relate to COP1 binding, we used AlphaFold2 to model the DET1-COP1 complex (*35*). We first modeled a 1:1 complex of DET1 with near full-length COP1, omitting the N-terminal 125 residues that are highly disordered in most predicted COP1 models. The highest scoring predictions showed COP1 binding to DET1 via its WD40 domain in two different modes (designated COP1′ and COP1″), each with low predicted aligned error (PAE) scores (<5 Å) for interface regions (fig. S5). PAE scores indicate the expected relative positional error between two residues, with lower values indicating higher confidence in interface predictions.

As both the COP1′ and COP1″ binding modes were largely compatible with each other, we tested modeling a single copy of DET1 bound with two copies of COP1. All 25 models of a 1:2 DET1:COP1 complex show a near-identical arrangement of the COP1 dimer bound to DET1, with correspondingly confident scores for both interface predicted template modeling (ipTM) and PAE of interface residues <5 Å (Fig. 3, A and B, and fig. S5). In these models, the COP1 WD40 domains occupy both binding sites identified in the 1:1 models, and the COP1 coiled-coil regions form an antiparallel arrangement. A dimeric COP1 protein mediated by the coiled coil is also suggested by assays showing that a COP1 RING-only construct has minimal activity in E2-ubiquitin discharge assays, whereas a longer construct including the coiled-coil domain had increased activity (Fig. 3C; residues 126 to 308; RING-COIL). Multiple angle light scattering shows that the COP1 RING domain (residues 126 to 208) forms weak, concentration-dependent dimers (fig. S5D), which we propose could be enhanced by coiled-coil dimerization. Yields of full-length COP1 precluded measurement of scattering data to confirm the stoichiometry of the DDD-COP1; however, the available data appear to be consistent with two COP1 molecules bound to DET1.

The two WD40 domains of the COP1 dimer bind to distinct interfaces on DET1 through nonequivalent regions of their WD40 domains (Fig. 3D). The first COP1 binding site on DET1 (COP1′) is adjacent to the Ube2e binding site and is primarily mediated by two loops from the COP1 WD40 domain. The second COP1 binding site (COP1″) is nearer the N-terminal portion of DET1 and is mediated by multiple different loops within the WD40 domain. The two DET1 binding sites are relatively comparable in area (1174 and 938 $Å^2$ for COP1′ and COP1″, respectively). However, both COP1 WD40-DET1 interfaces are substantially smaller than the area buried by the COP1 dimer interface within the complex (3242 $Å^2$). Although the precise details of the AlphaFold interfaces should be viewed conservatively, the overall characteristics are consistent with a COP1 dimer binding to DET1 through two asymmetric binding sites of DET1. The two COP1 binding interfaces predicted by AlphaFold are centered on a portion of DET1 (417 to 443) that is identical to the cryo-EM density of closed DET1 but not present in the open subclasses of DET1 (Fig. 2).

To test the AlphaFold2-based model of the DET1-COP1 complex, we designed mutations in the main loops of the COP1 WD40 domain that would affect each interface. We created multisite loop mutants in COP1′ (LY417DD and VLD686GSG) and COP1″ (QEHE510SSHS) and cotransfected with DET1 into Expi293 cells, along with wild-type COP1 (Fig. 3E). Wild-type COP1 levels were markedly reduced upon DET1 coexpression, compared to when COP1 was expressed alone. In contrast, COP1′ and COP1″ loop mutants were expressed at similar levels regardless of the presence of DET1. These results suggest that COP1 loop mutants behave differently in the presence of DET1, reflecting potential differences in recruitment to $CRL4^{DET1}$.

As coexpression markedly altered protein levels, we expressed COP1 and DET1 separately and then tested the ability of the mutants to copurify with DET1 (Fig. 3F). Mutation of COP1″ with a mutant lacking the QEHE (residues 510 to 513) loop markedly reduced the amount of DET1 copurified by COP1. In contrast, mutations in the COP1′ loops had a more moderate effect—the LY417DD mutant showed roughly wild-type pull-down, whereas the VLD686GSG mutant had reduced binding relative to wild-type COP1. Overall, this suggests that among the multifaceted binding sites, the COP1″ interface may be more important for DET1 binding, but mutation of either COP1′ or COP1″ loops can disrupt incorporation into $CRL4^{DET1\text{-}COP1}$ and degradation.

As the COP1″ binding site appeared to be most crucial to binding, we made single point mutations in the COP1″ loop and a point mutant in DET1 to dissect binding further (Fig. 3, D and G). Mutation of COP1 at Glu^{511} abrogated DET1 retention completely, whereas Glu^{513} did not affect binding (Fig. 3G), which is consistent with Glu^{511} being more central to the interface and Glu^{513} being slightly more peripheral. We then tested reciprocal mutation on the DET1 side of the interface (Y490D), which lies between Glu^{511} and Glu^{513} (Fig. 3, D and H). There was a marked decrease in DET1 Y490D binding to wild-type COP1 as compared to that of the wild-type DET1, consistent with the COP1″ binding site being an important determinant of COP1 recruitment to DET1. In the AlphaFold model, we also noted that the COP1 WD40 domain at the COP1′ site appears to interact with both DET1 and Ube2e2. Testing a single point mutant in COP1 that is oriented toward Ube2e2 (V458D) showed that the mutation reduced DET1 binding (Fig. 3G). This suggests that Val^{458} is also important for DET1-COP1 binding (Fig. 3D), although it is oriented toward the Ube2e binding site and not toward DET1 itself.

Together, mutagenic data are consistent with the AlphaFold model showing a COP1 dimer binding to DET1 through a multifaceted interface, including two asymmetric binding sites on DET1—that are available in the closed state of DET1—and further enhanced by a Ube2e enzyme.

DET1 closure regulates COP1 binding

The dynamic states suggested by cryo-EM and HDX-MS and the validated interfaces from AlphaFold2 together suggest a hypothesis that closed DET1 is integral to COP1 binding. A previous study has identified that substrate degradation by $CRL4^{DET1}$ is regulated by

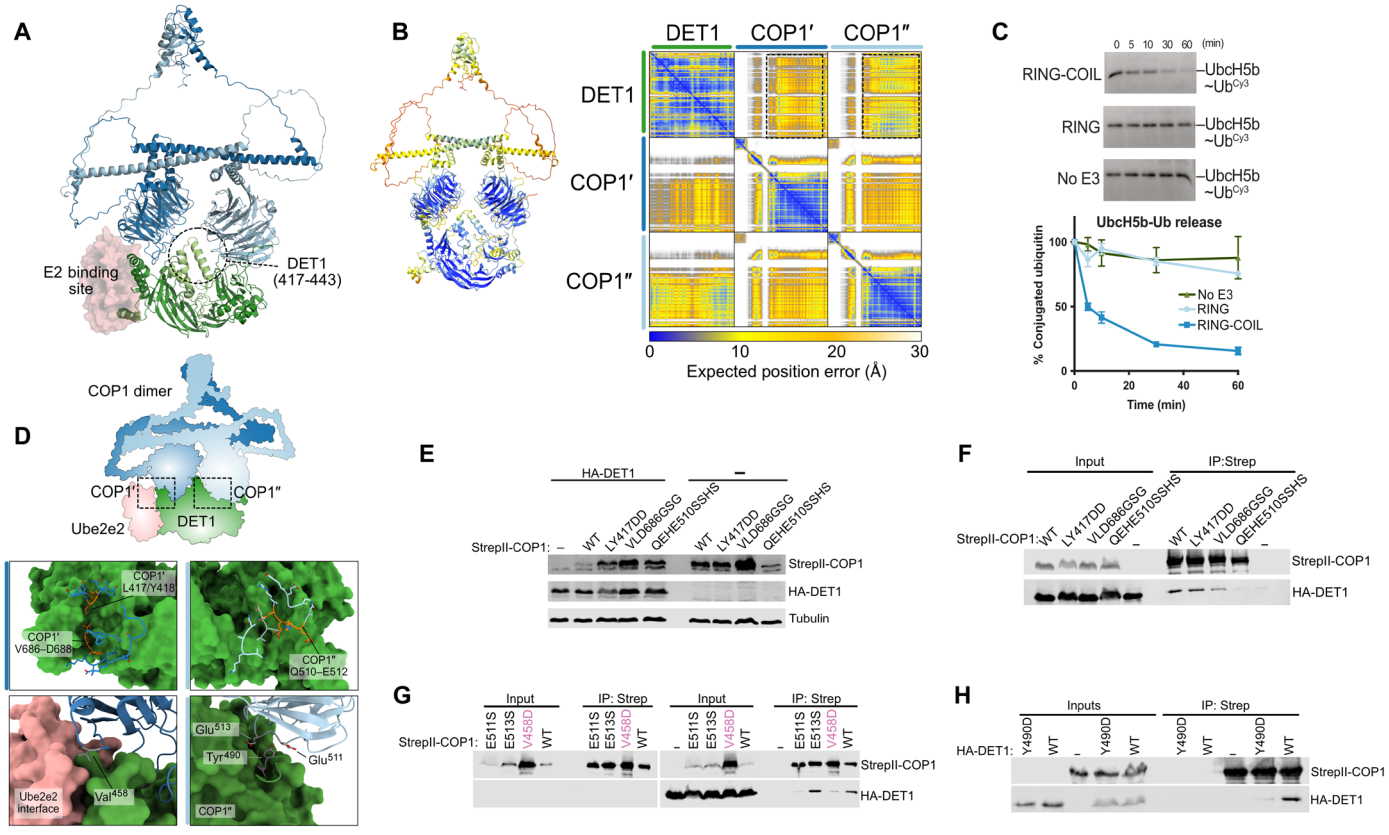

Fig. 3. COP1 binds DET1 through two asymmetric binding sites. (**A**) AlphaFold2 model of the 2:1 COP1-DET1 complex, indicating dynamic region of DET1 and E2-binding cup. (**B**) Overall Local Distance Difference Test (LDDT) scores (left) and PAE plot (right), relating to model shown in (A). (**C**) Ubiquitin is discharged by the COP1 RING-COIL but not the RING alone from UbcH5b. Ubiquitin discharge assays were used to determine the ability of COP1 RING or COP1 RING-COIL to cause ubiquitin discharge from UbcH5b. Samples were taken at 0, 15, 30, and 60 min, and ubiquitin discharge was determined by visualizing Cy3-ubiquitin. (**D**) Close-up views of the interface between DET1 and COP1 [COP1′ (left panels), COP1″ (right panels)]. (**E**) Coexpression of DET1 and COP1 in Expi293 cells shows destabilization of wild-type (WT) COP1 by DET1 but not by COP1′ or COP1″ mutants. Western blotting was performed to determine COP1 and HA-DET1 levels. (**F**) Multisite mutations show that the COP1″ interface is crucial for interaction with DET1. Western blot analysis was used to determine copurification of HA-DET1 by either WT COP1 or binding mutants [COP1 LY417DD, VLD686GSG (COP1′), or QEHE510SSHS (COP1″)] following affinity purification with Strep-TactinXT 4Flow resin. (**G**) Point mutations of COP1 show that Glu^{511} in the COP1″ site and COP1 Val^{458} (oriented toward Ube2e2) are crucial for COP1-DET1 binding. (**H**) DET1 mutant (Y490D) at the COP1″ interface has reduced COP1 binding. Western blot analysis was used to determine copurification of HA-DET1 by StrepII-COP1, either WT or binding mutants, following affinity purification with Strep-TactinXT 4Flow resin.

MAP kinases via two prominent phosphorylation sites on DET1—Ser^{66} and Ser^{458}—which modulate its ability to degrade substrates in cooperation with COP1 (*21*). Ser^{66} is located within the DET1-DDB1 interface and is likely to only be able to be phosphorylated when DET1 is dissociated from DDB1 (fig. S4D). To investigate how phosphorylation could affect the interaction between COP1 and DET1, we focused on Ser^{458}, which sits within the dynamic region of DET1 (Fig. 4A and fig. S4C). In the closed conformation, this region folds back onto itself to interact with the core of the molecule. Unphosphorylated Ser^{458} interacts with the loop containing Phe^{522} in the DET1 core. The tightly packed arrangement of the closed conformation would not be compatible with phosphorylation of Ser^{458}.

Targeting DET1 with mutations previously shown to affect ETV5 degradation (*21*), we directly measured COP1 recruitment. Immunoprecipitation of DET1 S458A by COP1 was similar to that of wild-type DET1. However, DET1 S458D was not bound by COP1 during copurification, suggesting that phosphorylation of Ser^{458} prevents DET1 from occupying the closed conformation and binding COP1 (Fig. 4, A and B). Two other rationally designed DET1 mutants at the closure interface (F408D and L463E) reduced, but did not completely abrogate, binding of COP1, indicating that the site of Ser^{458} is uniquely sensitive to disruption (Fig. 4, A and B). In combination with our structural data, this indicates that Ser^{458} phosphorylation can regulate COP1 incorporation into the larger CRL4$^{\text{DET1-COP1}}$ complex.

Probing other factors that may affect DET1 dynamics, we had noted correlation between closure of DET1 and DDA1 occupancy (Fig. 2, A and B), where DET1 classes that exhibit more of an "open" state had low DDA1 occupancy. In the closed state of DET1, the C-terminal helix of DDA1 interacts with DET1, but as DET1 moves toward the open form, the density for this helix becomes more disparate. The binding interface between DET1 and DDA1 is relatively minimal; therefore, we tested several DET1 mutants that interact at various points of the DDA1 helix (Fig. 4C). We expressed COP1 and DET1 separately in Expi293 cells and mixed the lysates of these, which would provide endogenous DDA1. Assessing the amount of DET1 copurified with COP1 showed that mutations that sit peripheral to the

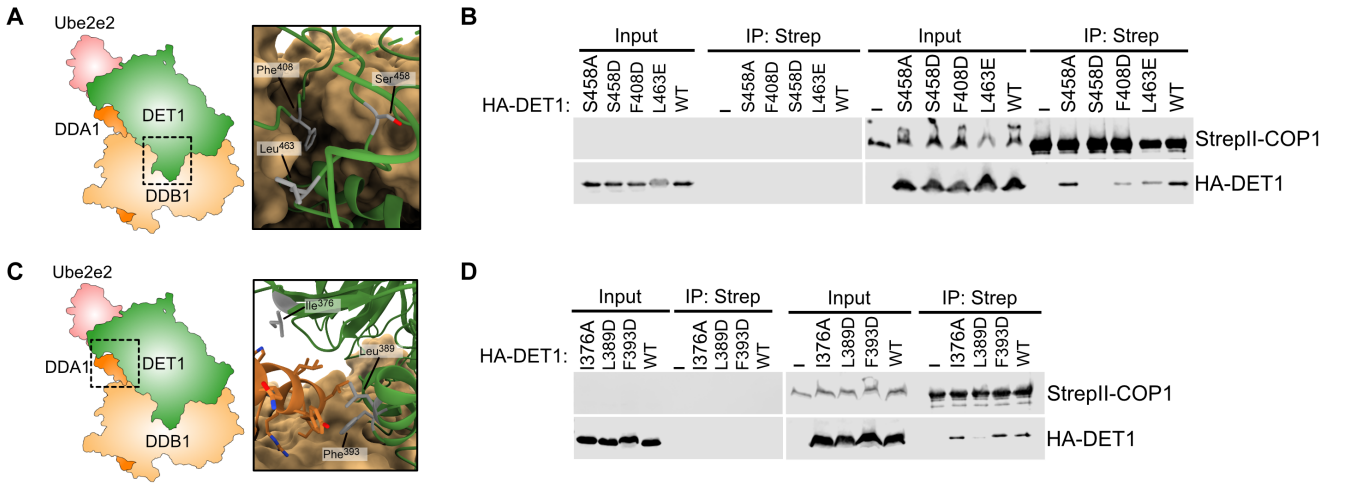

Fig. 4. Closure of DET1 is important for the COP1-DET1 interaction. Western blot analysis was used to determine copurification of either WT HA-DET1 or binding mutants by WT StrepII-COP1 following affinity purification with Strep-TactinXT 4Flow resin. (**A** and **B**) Mutation of DET1 S458 to a phosphomimetic residue (S458D) abrogates COP1-DET1 binding, whereas a nonphosphorylatable residue (S458A) binds efficiently, and mutating other residues at the interface have more minor effects. (**C** and **D**) Mutation that disrupts the coordination of the C-terminal DDA1 helix with DET1 (L389D) is sufficient to disrupt the binding of COP1 to DET1.

interaction site, I376A and F393D, did not affect DET1-COP1 binding (Fig. 4D), whereas L389D abrogated binding. Leu^{389} in DET1 acts to anchor the C-terminal helix of DDA1 and coordinates three residues near the start of the C-terminal helix of DDA1, Leu^{55}, Tyr^{58}, and Leu^{59} (Fig. 4C). These data suggest that DET1 closure can be controlled twofold—phosphorylation of Ser^{458} at the closure interface and stabilization by DDA1 may both contribute to the regulation of DET1 dynamics and subsequent COP1 binding.

The DET1 cup specifically binds Ube2e2

Having validated multiple interfaces that are important for COP1 binding to DET1, we turned to the functional implications of Ube2e recruitment by DET1. A segment composed of DET1 residues 263 to 291 mediates interactions toward the C terminus of the E2, whereas residues 292 to 329 form a helix-loop-helix arrangement that makes extensive contacts with the β sheet backside of Ube2e2 (Fig. 5A). Although previous analysis suggested that the N-terminal extension of the Ube2e family contributes to DET1 binding (*16*), the N-terminal tail was not observed in cryo-EM density. However, binding by the structurally conserved core of the catalytic domain raised the question of whether DET1 may also bind other ubiquitin-conjugating enzymes.

To test the specificity of this interaction between the Ube2e family and DET1, we compared the DET1 binding ability of a set of E2s. The E2s were chosen based on high sequence conservation to Ube2e2, including Ube2d2, Ube2n, Ube2k, and Ube2w (fig. S6A). In vitro pull-down experiments with this set of E2s showed clear specificity—only Ube2e2 was pulled down by the DDD complex (Fig. 5B). In parallel, AlphaFold2 multimer modeling showed remarkable DET1 specificity in line with experimental pull-down, with only human Ube2e1, Ube2e2, and Ube2e3 showing ipTM scores > 0.8 (fig. S6B) and high confidence PAE plots. Manual inspection of structures that had a high interface template modeling score (ipTM > 0.80) revealed complexes that superimpose well into cryo-EM density, whereas structures with ipTM < 0.80 showed E2 in the correct general area but in a variety of different arrangements (fig. S6C). This aligns well with previous observations that only the Ube2e family enzymes copurify with the DDD complex (*16*).

We also experimentally determined that the DET1 cup was required for DET1-E2 binding through glutathione *S*-transferase (GST) pull-down experiments with GST-tagged Ube2e2 (Fig. 5C). Pull-down of wild-type DET1 was observed, whereas a DET1 construct lacking the 263 to 327 cup (Fig. 5C, "Δ") was unable to be pulled down by Ube2e2, demonstrating that the cup is required for DET1-E2 binding. Binding to the DET1 cup would preclude backside ubiquitin binding of the E2, a mechanism previously observed to promote activity of canonical E2 enzymes (*36*–*38*). Assessing whether DET1 binding may itself promote Ube2e2-ubiquitin discharge failed to show activity, whereas discharge of Ube2e2 could be rapidly induced by a control E3 enzyme [RNF12 (*39*)] (Fig. 5D). This suggests that binding to the DET1 cup is not necessarily linked to the ubiquitin conjugation state of the Ube2e2 and may be indicative of a non-canonical role of the E2 within the complex.

Ube2e2 is a noncatalytic scaffold

In plants, the E2 protein that binds to DET1 (COP10) is catalytically inactive and cannot be charged (*13*, *40*). It is therefore plausible that, in humans, E2 binding to the DET1 cup may play a noncatalytic role in promoting complex formation. To test the consequences of E2 incorporation into CRL4$^{\text{DET1-COP1}}$ complexes, we cotransfected COP1 and either wild-type DET1 or the cup deletion mutant into Expi293 cells. When COP1 was cotransfected with the DET1 cup deletion mutant, COP1 was rescued from the degradation observed when wild-type COP1 and DET1 are overexpressed together (Fig. 5E). To assess the implications of the loss of the DET1 cup for COP1 binding, wild-type DET1 or the cup deletion mutant and COP1 were expressed separately in Expi293 cells, lysates were mixed, and copurification was assessed. The DET1 cup deletion mutant had severely reduced COP1 binding compared to wild-type DET1 (Fig. 5F). Narrowing these mutations, we saw that single point mutations within the cup—W304D and F320D—also markedly reduced DET1 binding by COP1 (Fig. 5, G and H). These results suggest that disrupting

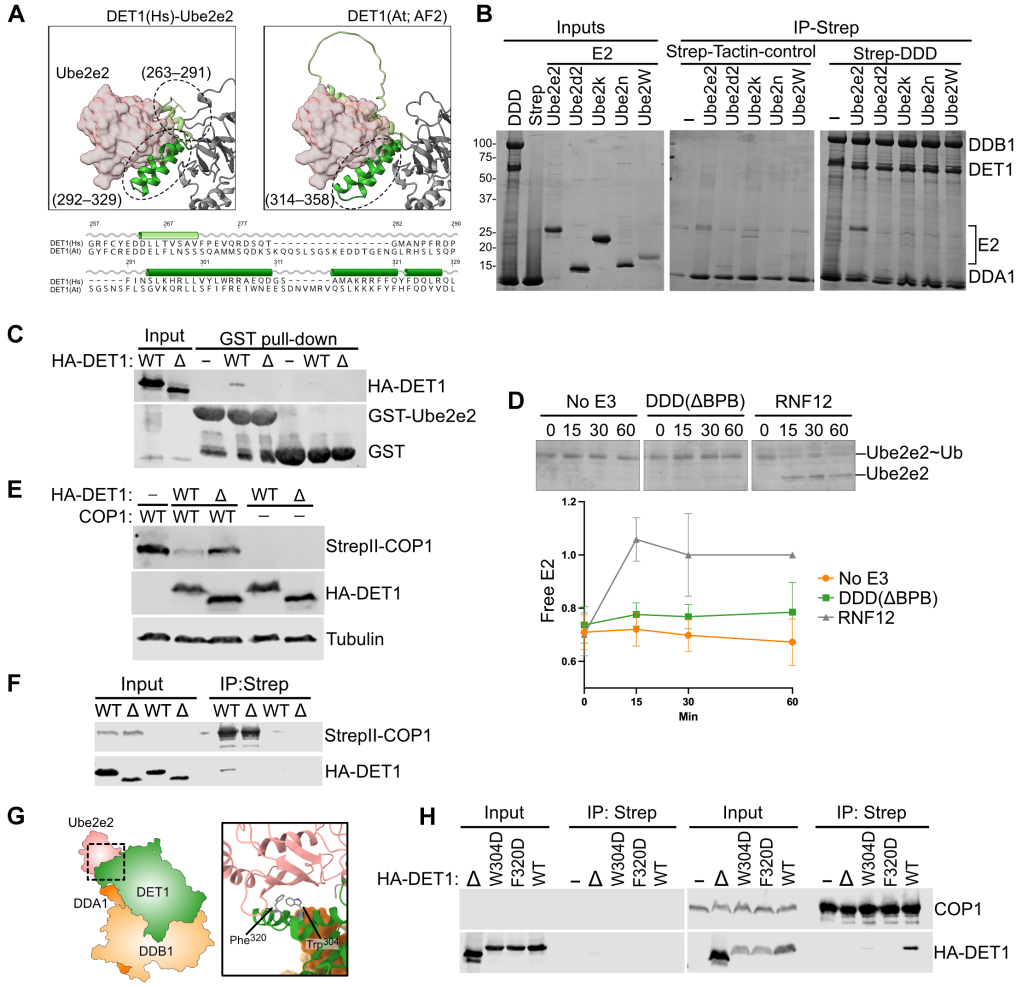

Fig. 5. Ube2e2 binding to DET1 is specific and important for DET1-COP1 binding. (**A**) AlphaFold2 modeling and sequence alignment of the human and Arabidopsis E2-binding loop of DET1 shows conservation of a helix-loop-helix, which mediates the interaction between DET1 and Ube2e2. (**B**) In vitro pull-down of E2 proteins by the DDD complex. Coomassie-stained gels showing pull-down of E2 proteins by the DDD complex immobilized on Strep-TactinXT resin. (**C**) GST pull-down of HA-DET1 by GST-Ube2e2. Western blot showing pull-down of HA-DET1 by GST-Ube2e2 immobilized on GSH resin shows that Ube2e2 binds full-length DET1 but not the "cup" mutant (Δ). (**D**) The DDD (ΔBPB) complex does not cause ubiquitin discharge from Ube2e2. Ubiquitin discharge assays were used to determine the ability of DDD to cause ubiquitin discharge from Ube2e2. Ubiquitin discharge was determined by staining gels with Coomassie blue. $N = 3$ technical replicates. (**E**) Wild-type COP1 is destabilized by full-length DET1 but not by the DET1 cup mutant. Coexpression of DET1 and COP1 in Expi293 cells shows destabilization of wild-type COP1 by DET1 but not by COP1′ or COP1″ mutants. (**F**) Pull-down of DET1 and DET1 cup deletion mutant (Δ) by COP1. COP1 interacts with full-length DET1 but not Δ-cup DET1. Copurification of HA-DET1 (either WT or Δ) by StrepII-WT COP1 following affinity purification with Strep-TactinXT 4Flow resin was assessed by Western blotting. (**G** and **H**) Single point mutations within the DET1 cup are sufficient to disrupt the interaction of DET1 to COP1. COP1 interacts with full-length DET1 but not DET1, which lacks the cup or has mutations at W304 or F320. Copurification of HA-DET1 (either WT, Δ, W304D, or F320D) by StrepII-WT COP1 following affinity purification with Strep-TactinXT 4Flow resin was assessed by Western blotting.

the ability of DET1 to recruit E2s has major effects on COP1-DET1 complex formation, consistent with Ube2e enzymes acting as a scaffold to aid DET1-COP1 binding.

Redirection of COP1 activity within CRL4$^{DET1\text{-}COP1}$

The role of two E3 ligases within a singular ubiquitin ligase complex remained perplexing. Thus, we used a combination of AlphaFold3 modeling and the structure of NEDD8-activated Cullin (CUL1) to model the architecture of activated CUL4 with both DDD and COP1 (*41*, *42*). The hybrid model clearly illustrates DET1 closure, and subsequent binding of COP1 would orient CRL4$^{DET1\text{-}COP1}$ well for ubiquitin transfer by CRL4 to substrates recruited by COP1 (Fig. 6A). Closed DET1 orients both substrate-binding pockets of COP1 toward the Rbx1 RING domain. The substrate-binding pockets of COP1′ and COP1″ are 70 and 57 Å, respectively, from the thioester bond of the charged active ubiquitin-conjugating enzyme bound to Rbx1 (*41*). Many COP1 substrates are transcription factors with relatively extended structures that could span this distance, but it remains to be determined whether further rearrangements are required for ubiquitin transfer.

To assess this model, we used multiturnover ubiquitin assays to probe the role of each of the components of the CRL4$^{DET1\text{-}COP1}$ complex. We first validated activity of recombinant COP1 in multiturnover ubiquitination assays, showing extensive autoubiquitination

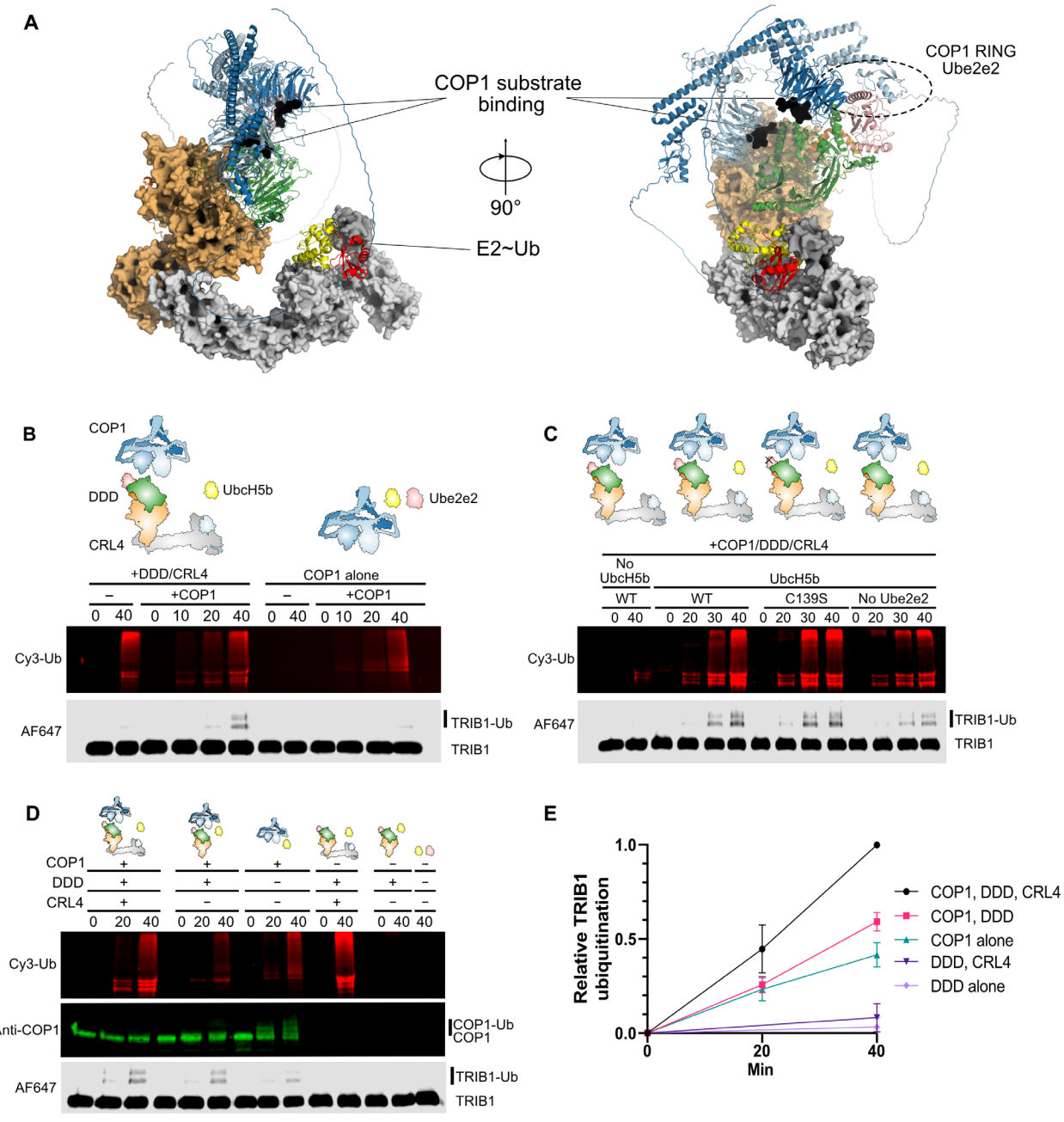

Fig. 6. Activity and regulation of COP1 activity. (**A**) Hybrid model of the CRL4$^{DET1\text{-}COP1\text{-}Ube2e2}$ complex. Created by sequential superposition of an AlphaFold3 model of DDD-COP1-Ube2e2 with active CUL1 [Protein Bank (PDB) 6ttu] and COP1-domain bound to TRIB1 peptide (PDB 5igo). The low–Local Distance Difference Test (LDDT) tail of Ube2e2 is omitted for clarity, E2~Ub shown in yellow-red, and substrate binding site of COP1 in black. (**B** to **D**) Multiturnover assays of CRL4$^{DET1\text{-}COP1}$ chain building. Samples were taken at 0, 10, 20, and 40 min, and ubiquitin chain formation was determined by visualizing the incorporation of Cy3-labeled ubiquitin onto TRIB1 (84 to 372) labeled with AF647. (B) DDD-CRL4 enhances ubiquitination of TRIB1 (84 to 372) by COP1. TRIB1 ubiquitination is increased when both CRL4^{DET1} and COP1 are present relative to COP1 or CRL4^{DET1} alone. (C) CRL4$^{DET1\text{-}COP1}$ is active with UbcH5b but not Ube2e2. (D) CRL4^{DET1} enhances COP1 ubiquitination of TRIB1 while stabilizing COP1 from autoubiquitination. COP1 levels are assessed during multiturnover assays by anti-COP1 immunoblotting. (**E**) Quantification of substrate ubiquitination by COP1, COP1-DDD, and COP1-DDD-CRL4 [quantification of (D), $N = 3$ technical replicates].

with UbcH5b, a promiscuous E2, but no activity with Ube2e2 (fig. S7A). We then assessed the ability of COP1 to transfer ubiquitin onto a model substrate—TRIB1. TRIB1 is a known substrate adapter for COP1, but itself is also subject to COP1-dependent degradation (*43*). Our recombinant TRIB1 construct (84 to 372) contained three potential ubiquitination sites but is missing a putative N-terminal ubiquitination site, Lys^{46} (*43*, *44*). COP1 alone had minimal activity on recombinant TRIB1, whereas the neddylated $CRL4^{DET1\text{-}COP1}$ complex showed increased TRIB1 ubiquitination (Fig. 6B). Because those assays contained both wild-type UbcH5b and Ube2e2, we tested whether altering the E2 complement of the complexes affected ubiquitination (Fig. 6C). TRIB1 ubiquitination was entirely dependent on active UbcH5b and reduced in the absence of Ube2e2, consistent with increased DET1-COP1 scaffolded by Ube2e2. The active site Ube2e2 C139S mutant showed similar substrate ubiquitination to wild-type Ube2e2, consistent with the scaffolding role of Ube2e2 being noncatalytic.

Tracking Cy3-ubiquitin showed that both $CRL4^{DET1}$ and COP1 in isolation had a tendency to autoubiquitinate in an in vitro format (Fig. 6). To simultaneously track the balance of autoubiquitination and TRIB1-substrate ubiquitination, we immunoblotted for COP1 in separate assays containing COP1, CRL4, the DDD complex, or combinations thereof. It was apparent that optimal TRIB1 ubiquitination occurs when the entire $CRL4^{DET1\text{-}COP1}$ complex is present, and TRIB1 ubiquitination is completely COP1 dependent. Within $CRL4^{DET1\text{-}COP1}$ assays, COP1 levels are relatively stable as monitored by immunoblotting (Fig. 6D, left). Notably, inclusion of only the DDD without CRL4 also appears to stabilize COP1 from autoubiquitination, whereas COP1 alone with TRIB1 substrate readily ubiquitinates itself and shows minimal TRIB1 ubiquitination (Fig. 6D, middle). Notably, this contrasts with cellular assays overexpressing wild-type DET1 and COP1 without substrate, where COP1 was destabilized (Figs. 3 and 5). Together, this suggests that the DDD complex can suppress COP1 autoubiquitination while recruiting it into the larger $CRL4^{DET1}$ complex, but in the cellular context, the balance of substrate, COP1, and DET1 levels is likely to be important determinants of the ultimate ubiquitination target.

DISCUSSION

Among the myriad of eukaryotic ubiquitin E3-ligases, Cullin-RING ligases recruit diverse substrates by building a modular system upon a common core. DCAF proteins provide diversity of Cullin-4 substrate recruitment when they are recruited via DDB1 and are particularly relevant to transcriptional regulation and DNA damage responses. Of the DCAF proteins, DET1 is somewhat enigmatic, given that its primary reported functions have been inhibition of CRL4 ubiquitination, binding to E2-ubiquitin–conjugating enzymes (*16*), and recruitment of another E3 ligase protein to CRL4 complexes, namely, COP1. Here, we describe the molecular architecture of DDB1-DDA1-DET1-E2 complexes and characterize a model for recruitment of COP1 to $CRL4^{DET1}$ complexes.

One of the most intriguing aspects of DET1 is its ability to recruit additional E2 enzymes to CRL4 complexes. This function appears to be unique among DCAF proteins reported to date. Published data and our analysis suggest that specific recruitment of Ube2e enzymes is mediated by a helical hairpin extending from DET1 that binds the backside β sheet of Ube2e2, here described as the DET1 "cup." The binding site for DET1 on Ube2e2 clearly precludes backside binding of ubiquitin (*36*, *37*), which activates ubiquitin transfer of other E2 enzymes. We did not observe enhancement of ubiquitin discharge from Ube2e2 by DET1 in up to an hour, suggesting that backside binding alone is not activating, a conclusion supported by the lack of substrate ubiquitination from Ube2e2 in any of our ubiquitination assays. This was observed no matter whether COP1 or the whole $CRL4^{DET1\text{-}COP1}$ complex was present, as long as Ube2e2 was the only E2 enzyme present within the reaction (Fig. 5D and fig. S7).

Instead, it appears that Ube2e2 coordinates the interface between COP1 and DET1. Ube2e enzymes preferentially catalyze monoubiquitination over polyubiquitination, although they avidly bind to BRCA1-BARD1 (*45*). The Ube2e N-terminal extension has been shown to impede extended ubiquitin chain building and acts as a target of autoubiquitination that limits activity (*46*–*48*). Moreover, the plant homolog of DET1 recruits a catalytically dead E2 enzyme (COP10), containing a serine rather than cysteine in its active site (*49*, *50*). Mutating the active site cysteine of Ube2e2 (C139S) does not affect the chain-building capability of $CRL4^{DET1\text{-}COP1}$ complex (Fig. 6C and fig. S7). Mutating residues that make contacts with Ube2e2 on either DET1 or COP1 impedes the DET1-COP1 interaction (Figs. 3 and 5). We propose that the Ube2e family E2s are not primarily required for building of ubiquitin chains by COP1 but rather act to recruit COP1 to DDD complexes. This mechanism offers an intriguing parallel between the human and the plant DET1-COP1 systems: In plants, the E2 recruited by DET1 is an obligate noncatalytic partner, whereas in humans, Ube2e2 appears to play a noncatalytic role, although it has a catalytic cysteine. This expands the role of E2 enzymes, which have already been demonstrated to regulate ubiquitination by driving substrate specificity in concert with substrate recruitment modules and managing the switch between priming and extension of ubiquitin chains (*38*, *51*, *52*). Here, Ube2e2 functions to modulate the assembly of a larger E3 complex.

Cryo-EM and HDX-MS analysis of the DDD complex demonstrated the dynamic nature of DET1 and the complex as a whole (Fig. 2), whereas phosphomimetic mutagenesis provided insight into how phosphorylation may affect complex formation (Fig. 4). This extends the paradigm of Cullin substrate adapter proteins being more than static substrate recruitment modules but function as dynamic and active players in ubiquitination. A study has shown that the substrate adapter protein Cereblon, a target of CELmod compounds and a range of proteolysis targeting chimera molecules, exists across a spectrum of conformations that can be biased by small molecules (*29*). Furthermore, DCAF1 mediates assembly of massive tetrameric CRL4 complexes, which have low activity but become active when substrate binding promotes dissociation into dimeric structures (*4*). In the case of DET1, the fully closed state presents two asymmetric binding sites that we propose mediate COP1 binding, in concert with the presence of Ube2e enzymes (Fig. 3). The fully closed structure of DET1 also correlates with stabilization of the C-terminal helix of DDA1. DDA1 resides in a similar location to that observed in multiple structures reported of DCAF15 bound to DDB1 (*30*, *31*). Although this has not been systematically reported, this may mean that DDA1 is also required for stabilization of substrate bound DCAF15. Beyond DCAF15, the only other DCAF-DDB1 structures incorporating DDA1 is that of DCAF16 (*53*, *54*). In those structures, only the N-terminal portion of DDA1 is visible bound to the BPC WD40 domain, if at all. Moreover, DCAF16 appears poorly disposed to interact with DDA1. It will be important in the future to systematically ascertain which DCAF

complexes DDA1 is an integral component of and how DDA1 may modulate the function of respective DCAF conformations and compositions.

The model we present here for COP1 recruitment to $CRL4^{DET1}$ sees a dimeric COP1 complex recruited to a monomeric DET1 protein through two asymmetric binding sites. Although AlphaFold2 also confidently allows for 1:1 complexes, the extended COP1 coiled-coil interface, that COP1 RING dimers are more active, and both 1:1 binding modes being compatible within a 2:1 complex all argue in favor of a 2:1 complex as the default oligomeric state. Within this complex, it appears unlikely that COP1 RING dimers would be favored to come together into their active state, especially if one of the RING domains is bound to a Ube2e enzyme as observed in several AlphaFold3 models (Fig. 6A). Prediction of the $CRL4^{DET1\text{-}COP1}$ complex structure placed one of the COP1 RING domains adjacent to the RING binding surface of Ube2e2—~27 Å from the end of the coil to the E2 binding site, which could be comfortably bridged by the RING-COIL linker. The other RING domain would instead have to span 120 Å from the predicted end of the coil to reach the E2 binding site, which makes RING dimerization less favorable. The $CRL4^{DET1\text{-}COP1}$ complex is more active than COP1 alone (Fig. 6C). If the RING domains are sequestered by binding to Ube2e2, COP1 may not function as an active E3 enzyme within the complex. However, overall substrate-targeted ubiquitination is enhanced. A COP1 dimer binding to DET1 would present two WD40 domains with binding sites for substrates or further substrate adapters such as the Tribbles pseudokinases (*20*, *55*–*57*). Reported COP1 substrates include multiple dimeric transcription factors (for example, P53, C/EBP family, and Jun transcription factors). A dimeric ligase recruiting dimeric substrates presents an attractive matching stoichiometry. The role of Tribbles proteins as further substrate adapters within such complexes could offer a mechanism to introduce further diversity. This suggests a mechanism by which COP1 autoubiquitination can be suppressed within the larger $CRL4^{DET1\text{-}COP1}$ complex, where its role is restricted to that of a substrate recruitment module.

The $CRL4^{DET1\text{-}COP1}$ complex appears unique in containing not only two E2 enzymes, one of which has a noncanonical function, but also two E3 enzymes to target substrates for ubiquitination. Despite the important roles of COP1 substrates in differentiation and development of multiple cell types, targeted proteomic studies have shown that DET1 and COP1 are among the least prevalent DCAF proteins resident within Cullin-4–DDB1 complexes (*58*). This may mean that $CRL4^{DET1\text{-}COP1}$ complexes act to tune wider functions of COP1, or vice versa. Having two E3 enzymes in one complex creates a unique opportunity for two enzymes to not only function together to direct substrate targeting but also regulate each other. CRL4 is an efficient E3 but does not have any intrinsic substrate recruitment activity and requires substrate adapters, such as the DCAF proteins (*28*). On the other hand, multiturnover assays indicate that isolated COP1 readily ubiquitinates itself, but it is not very efficient at targeting TRIB1 as a substrate. Incorporation of COP1 into the $CRL4^{DET1\text{-}COP1}$ can shift the balance of ubiquitination toward TRIB1 and suppress COP1 autoubiquitination. Protein abundance, localization, and concentration will be crucial to this balance, given that overexpression in cells without elevated substrates leads to COP1 degradation by $CRL4^{DET1}$(Figs. 3E and 5E). Further complexity may arise because TRIB1 is a substrate and a substrate adapter for other transcription factors (*43*, *55*), and our model TRIB1 substrate lacks potentially relevant ubiquitin target sites. Thus, this model provides a starting point, with multiple further aspects that remain to be clarified to fully understand regulation of substrate degradation in cellular settings at endogenous levels.

Overall, the data described here provide a clear architecture upon which to interpret multiple modes of COP1 function and relationship to larger $CRL4^{DET1}$ complexes. Although incorporation into the DDD complex may be a general mechanism to protect COP1 from autoubiquitination, the balance of protein and substrate adapters is likely to play a major role in the eventual targets of ubiquitination. Whether specific transcription factor substrates, or substrate adapters, are primarily targeted by COP1 alone or the $CRL4^{DET1\text{-}COP1}$ complex remains as a key outstanding question, which will be crucial to transcriptional programming of multiple cell types.

MATERIALS AND METHODS

Plasmids and cloning

DNA constructs for recombinant protein expression were amplified to incorporate the 5′-(CAGGGACCCGGT) and 3′-(TAACCGGGCTTCTCCTCG) overhangs, required for ligation-independent cloning (LIC). TRIB1 (84 to 372), COP1 RING (126 to 208), and COP1 RING-COIL (126 to 308) were cloned into a modified pET-LIC vector incorporating an N-terminal His_6 tag and a 3C protease cleavage site for expression in *Escherichia coli* BL21 (DE3). Plasmids encoding the various proteins required for ubiquitination, including the Ube1 (E1), various E2s, and ubiquitin, were provided by the Day Lab (University of Otago). Plasmids encoding the various proteins required for neddylation, including the UBA3/APPBP1 and Nedd8, were acquired from MRC PPU Reagents (DU61958 and DU32475). Cul4A was cloned into a pFastBac expression vector modified to incorporate an N-terminal affinity tag followed by a 3C protease cleavage site, and Rbx1 was cloned into the pFastBac expression vector modified to incorporate an N-terminal StrepII tag followed by a 3C protease cleavage site.

To generate a coexpression construct for the DDD complex, full-length open reading frames encoding DET1, DDB1, and DDA1 were cloned into a pFastBac expression vector modified to incorporate an N-terminal affinity tag followed by a 3C protease cleavage site. DDB1 and Ube2e2 were cloned to include an N-terminal His_6 tag, DET1, and N-terminal StrepII tag, and DDA1 remained untagged. These were then reamplified and assembled into coexpression complexes in pBig1a using Gibson assembly (*59*). An additional construct was produced in which the BPB of DDB1 was removed (Δ396 to 706; ΔBPB) in the same manner.

To generate bacmid constructs, either pFastBac or pBig1a coexpression constructs were transformed into DH10EMBacY cells (Geneva Biotech) and screened to identify constructs containing all the complex components. The isolated bacmids were transfected into *Spodoptera frugiperda* cells and used to produce baculoviral stocks, which were then used for subsequent protein expression.

DNA constructs for protein expression in Expi293F (Thermo Fisher Scientific) were produced as follows: Full-length COP1was cloned into a modified pcDNA3.1 expression vector modified to incorporate an N-terminal StrepII tag and DET1 into the equivalent vector with an N-terminal hemagglutinin tag. The DET1 cup mutant (Δ) was generated by a two-step overlap polymerase chain reaction and cloned into the same base vector as the full-length construct. Mutations in DET1, COP1, and Ube2e2 were introduced by site-directed mutagenesis.

Expression and purification of recombinant protein

Purification of proteins expressed in E. coli

Bacterial constructs [TRIB1 (84 to 372) and COP1 RING (126 to 208)/RING COIL (126 to 308)] and the proteins involved in the ubiquitin and neddylation cascades were expressed in *E. coli* BL21 (DE3) cells. Cells were grown at 37°C in Luria-Bertani medium to an OD_{600} (optical density at 600 nm) of ~0.6 and then induced with 0.2 mM isopropyl-β-D-1-thiogalactopyranoside and grown at 18°C overnight. Bacterial constructs were expressed with His_6 tags, except for Ubc12, which has a GST tag. His_6 proteins were purified using Ni^{2+} affinity resin [His-Select resin (Sigma-Aldrich)], whereas GST-tagged Ubc12 was purified using GSH resin. Cell pellets were resuspended in purification buffer [50 mM tris-HCl (pH 8.0), 300 mM NaCl, 10 mM imidazole, 10% (v/v) glycerol, and 10% (w/v) sucrose]. Cells were lysed via sonication, and the soluble fraction was purified using affinity resin. Proteins were eluted from the resin by increasing the imidazole concentration to 300 mM. Ubc12 was purified using GSH resin and eluted with glutathione. Ubiquitin was expressed as an untagged protein and then purified and labeled with Cy3 as per (*60*).

Proteins required for fluorescence labeling were dialyzed into phosphate-buffered saline (PBS) (pH 8.0) and labeled using the Alexa Fluor 647 Protein Labeling Kit [A20173 (Thermo Fisher Scientific)]. Labeled protein was then snap frozen in liquid nitrogen and stored at −80°C.

Production of full-length COP1

Full-length COP1 was expressed in Expi293F cells. Expi293F were grown in Expi293 Expression Medium (Gibco, A1435102) supplemented with penicillin-streptomycin (100 U/ml; Life Technologies, 15140122). Cells were grown at 37°C in a humidified atmosphere with 8% CO_2, shaking at 120 rpm.

Cells were transfected with ExpiFectamine293. ExpiFectamine293 Transfection Enhancer 1 and ExpiFectamine293 Transfection Enhancer 2 were added to the transfection flask 18 to 22 hours posttransfection. Cells were harvested 72 hours posttransfection by centrifugation at 1000*g* for 30 min, washed with PBS, and then repelleted. Pellets were snap frozen in liquid nitrogen.

Cells were lysed via sonication, and the soluble fraction was purified by affinity chromatography using Strep-TactinXT 4Flow resin. Resin with COP1 bound was washed in PBS, and then the protein was eluted using 100 mM PBS (pH 7.0) containing 50 mM biotin. If required, COP1 was then dialyzed overnight to remove the biotin.

Purification of the DDD complex

The DET1-DDB1-DDA1 complex was produced as either a complex containing full-length DDB1 or with DDB1 lacking its central WD40 domain (ΔBPB). For initial cryo-EM structure, the full-length complex had Ube2e2 coexpressed. For the DDD(ΔBPB) structure, Ube2e2 was expressed separately in *E. coli* and added in excess to the DDD complex, then the whole complex was further purified.

The full-length DDD complex (full-length DDB1, DET1, and DDA1) was produced in *Trichoplusia ni* (TNi). Cells were incubated with baculovirus at 28°C for 48 hours. Full-length DDD-Ube2e2, which was used for the initial cryo-EM structure, was produced in *S. frugiperda* (SF9) at 27°C. Cells were incubated with baculovirus at 28°C for 72 hours. DDD(ΔBPB) was produced in *S. frugiperda* (SF9) at 22°C [full-length DET1 and DDA1 (DDD(ΔBPB)]. Cells were grown at 27°C until the addition of baculovirus at which point the temperature was reduced to 22°C for 96 hours. Following incubation with baculovirus, cells were harvested by centrifugation at 1000*g* for 30 min.

Cell pellets were resuspended in purification buffer [50 mM tris-HCl (pH 8.0), 300 mM NaCl, 10% (v/v) glycerol, and 10% (w/v) sucrose]. Cells were lysed via sonication, and the soluble fraction was purified by affinity chromatography using Strep-TactinXT 4Flow resin (IBA Lifesciences). Using a gravity flow column, clarified lysates were purified by affinity chromatography, the bound resin was washed with 50 mM tris-HCl (pH 8.0) and 150 mM NaCl and then the protein was eluted from the resin with a wash buffer containing 50 mM biotin.

The full-length DDD required for multiturnover assays was purified by affinity purification and then buffer exchanged into 50 mM tris-HCl (pH 8.0) and 150 mM NaCl. If further purification was required, this was done by size exclusion chromatography using either a Superdex200 Increase 10/300 column (GE Life Sciences) or a Superose6 Increase 10/300 Column (GE Life Sciences). The initial full-length DDD complex for EM was purified in 50 mM tricine (pH 8.0), 80 mM NaCl, and 0.5 mM tris(2-carboxyethyl)phosphine (TCEP). Subsequent purifications of either full-length or DDD(ΔBPB) used 50 mM tris-HCl (pH 8.0) and 150 to 300 mM NaCl. Purified protein was snap frozen in liquid nitrogen and stored at −80°C until required.

Purification of CUL4/Rbx1

Cul4A/Rbx1 (CRL4) was produced in *S. frugiperda* (SF9) at 27°C. Baculoviruses for each of these proteins were produced separately. Cells were incubated with both baculoviruses and incubated at 28°C for 72 hours. Following incubation with baculovirus, cells were harvested by centrifugation at 1000*g* for 30 min.

Cell pellets were resuspended in purification buffer [50 mM tris-HCl (pH 8.0), 300 mM NaCl, 10% (v/v) glycerol, and 10% (w/v) sucrose]. Cells were lysed by sonication and clarified by centrifugation, and the Cul4/Rbx1 was initially purified using Ni^{2+} affinity [His-Select resin (Sigma-Aldrich)] and then dialyzed overnight into 20 mM Hepes (pH 7.6) and 200 mM NaCl. Cul4A was then neddylated.

Neddylation of Cul4A

Dialyzed Cul4A was neddylated by incubating 2 μM Cul4A/Rbx1 with 0.15 μM UBA3, 1 μM Ubc12, and 30 μM Nedd8, in a buffer containing 20 mM Hepes (pH 7.6), 200 mM NaCl, 2.5 mM $MgCl_2$, 5 mM dithiothreitol (DTT), and 1.25 mM adenosine triphosphate (ATP). Samples were incubated at room temperature for 1 hour. The neddylated Cul4A/Rbx1 complex was then further purified using Strep-TactinXT 4Flow resin. Purified protein was snap frozen in liquid nitrogen and stored at −80°C until required.

Electron microscopy and structure determination

For full-length DDB1-DET1-DDA1-Ube2e2, glow-discharged 300-mesh C-Flat 1.2/1.3 grids (Protochips) were placed in Vitrobot MarkIV (Thermo Fisher Scientific) at 4°C and 100% relative humidity. Three microliters of protein sample at a concentration of 0.6 mg/ml in 50 mM tricine (pH 8.0), 8 mM NaCl, and 0.5 mM TCEP was applied to the grids and blotted for 8 s with blot force 4 before plunge freezing in liquid ethane. A total of 4957 micrographs were collected using a Titan Krios microscope (Thermo Fisher Scientific) operated at 300 kV. Micrographs were recorded using EPU with a K2 summit (Gatan) camera at calibrated pixel size 0.66 Å/px and 0.8- to 2-μm underfocus. The total dose of 66 e/$Å^2$ was fractionated over 60 frames.

Processing was carried out in Cryosparc v 3.0.1, unless specified otherwise (*61*). Movies were aligned patchwise and binned 2 by 2. Contrast transfer functions (CTFs) of the aligned micrographs were determined patchwise. Blob picking and 2D classification yielded templates for template-based picking, where further 2D classification and selection gave a dataset of 550k particles. Rounds of 2D and 3D classification yielded a set of 221k particles, which were refined in nonuniform refinement to 3-Å resolution. The micrographs were motion corrected in a full-frame manner, and full-resolution particles with per particle, local motion correction were then reconstructed in a nonuniform refinement to a resolution of 2.89 Å —but which suffered from severe map anisotropy. Processing in parallel using 3D classifications, multibody refinements, or focused classifications and refinements in RELION 3.1.2 (*62*) did not improve map clarity. The final map from Cryosparc was postprocessed using deepEMhancer (*63*), and its sphericity, global, and directional resolution was estimated using 3DFSC (*64*).

The DDD (ΔBPB) complex was concentrated, mixed with an excess of Ube2e2, and then repurified using an S200 Increase 5/150 in 50 mM tris-HCl (pH 8.0) and 300 mM NaCl. Fractions containing the whole complex were pooled and then concentrated to ~0.85 mg/ml before cryo-EM. Samples for collection were placed on Quantifoil 1.2/1.3 grids in a Vitrobot MarkIV (Thermo Fisher Scientific) at 10°C and 100% relative humidity. Three microliters of protein sample was applied to the grids and blotted for 5 s before plunge freezing in liquid ethane. A total of 14,499 micrographs were collected using a Titan Krios microscope (Thermo Fisher Scientific) operated at 300 kV. Micrographs were recorded using EPU equipped with a BioQuantum energy filter (Gatan) (15 eV) and a K3 direct detection camera (Gatan) at a calibrated pixel size of 0.65 Å/px and −1.0-μm underfocus. The total dose of 80 e/Å^2 was fractionated over 100 frames. Processing was carried out mainly in Cryosparc v4.3.1, with some later processing using versions up to v4.4.1+. Movies and CTFs were aligned patchwise. Blob picking and 2D classification yielded templates for template-based picking, where further 2D classification and selection yielded 1.9 million particles. Rounds of 3D classification yielded a set of 375k particles, which were then further divided through 3D variability analysis using a mask of the whole complex. This yielded a set of 63k particles, which were refined in nonuniform refinement to 3-Å resolution. The micrographs of those particles were reextracted at a larger box size before local and global CTF refinement was performed. Reference-based motion correction was performed on the exposures that yielded those particles before a final nonuniform refinement was performed, resulting in a set of 61,234 particles yielding a resolution of 2.83 Å. Structural determination was performed iteratively using Phenix and Coot to fit the structural model to the map refined in Cryosparc. With the exception of Cryosparc, structural biology software was compiled by SBGrid (*65*).

AlphaFold modeling

AlphaFold2 modeling was performed on the high-performance computing cluster at the University of Otago. Models of DET1-COP1 binding were generated using AlphaFold2-Multimer (*35*, *66*) based on full HHblits alignment protocols implemented in https://github.com/google-deepmind/alphafold, with max_template_date=2020-05-14, model_preset=multimer, and five predictions per model. The N-terminal 125 amino acids of COP1, which are suggested to be completely disordered in full-length AlphaFold models, were omitted from predictions. Models of E2 enzymes in complex with DET1 were generated using full-length DET1, the full-length or full-length human sequences of Ube2e2, or core catalytic domains of other E2 enzymes as displayed in the alignment in fig. S6. Top models of COP1-DET1 or DET1-E2s were ranked based on the ipTM score, a score that represents the confidence in the interfaces within the model. The highest scoring models, or summary data corresponding to ipTM scores, are represented in the manuscript. PAE scores were plotted beside each the model; these scores indicate the expected relative positional error between two residues. Lower values indicate a higher confidence interface, with blue being indicative of high confidence and yellow of low.

HDX-MS sample preparation

HDX reactions measuring the rate of hydrogen-deuterium exchange across the DDD (ΔBPB) complex were carried out in a 40-μl reaction volume containing 16 pmol of protein [DDD (ΔBPB)]. The exchange reactions were initiated by the addition of 32 μl of D_2O buffer [20 mM Hepes (pH 7.5), 150 mM NaCl, 0.5 mM TCEP, and 95.1% D_2O (v/v)] to 8 μl of protein (final D_2O concentration of 76.1%). Reactions proceeded for 3 s at 0°C before being quenched with ice cold acidic quench buffer, resulting in a final concentration of 0.6 M guanidine HCl and 0.9% formic acid postquench. Samples were created and run in independent triplicate. Samples were flash frozen immediately after quenching and stored at −80°C until injected onto the ultraperformance liquid chromatography (UPLC) system for proteolytic cleavage, peptide separation, and injection onto a Quadrupole Time-of-Flight (QTOF) for mass analysis, described below.

A fully deuterated sample was made by incubating 4 μl of 4 μM DDD (ΔBPB) with 4 μl of 3 M guanidine HCl (to achieve a final concentration 3 M), for 5 min at 20°C, followed by the addition of 32 μl of D_2O buffer [20 mM Hepes (pH 7.5), 150 mM NaCl, 0.5 mM TCEP, and 95.1% D_2O (v/v)]. Reactions proceeded for 10 min at 50°C, then 2 min at 20°C, and then 0°C for 2 min before being quenched as above. Samples were flash frozen immediately after quenching and stored at −80°C.

Protein digestion and tandem mass spectrometry data collection

Protein samples were rapidly thawed and injected onto an integrated fluidics system containing a HDx-3 PAL liquid handling robot and climate-controlled (2°C) chromatography system (LEAP Technologies), a Waters Acquity UPLC I-Class Series System, and an Impact HD QTOF mass spectrometer (Bruker). The full details of the automated LC system were previously described in (*67*).

The samples were run over an immobilized pepsin column (Affipro; AP-PC-001) at 200 μl/min for 4 min at 2°C. The resulting peptides were collected and desalted on a C18 trap column [Acquity UPLC BEH C18 1.7 μm column (2.1 mm by 5 mm); Waters 186004629]. The trap was subsequently eluted in line with an ACQUITY 300 Å, 1.7-μm particle, 100 mm–by–2.1 mm BEH C18 UPLC column (Waters), using a gradient of 3 to 10% B (Buffer A 0.1% formic acid; Buffer B 100% acetonitrile) over 1.5 min, followed by a gradient of 10 to 25% B over 4.5 min, followed by a gradient of 25 to 35% B over 5 min, then was maintained for 1 min at 35% B, and lastly a gradient of 35 to 80% B over 1 min was used. Mass spectrometry experiments acquired over a mass range from 150 to 2200 mass/charge ratio (*m*/*z*) using an electrospray ionization

source operated at a temperature of 200°C and a spray voltage of 4.5 kV.

Peptide identification

Peptides were identified from the nondeuterated samples of DDD(ΔBPB) using data-dependent acquisition following tandem mass spectrometry (MS/MS) experiments (0.5-s precursor scan from 150 to 2000 *m*/*z*; 12 0.25-s fragment scans from 150 to 2000 *m*/*z*). MS/MS datasets were analyzed using FragPipe v18.0, and peptide identification was carried out by using a false discovery–based approach using a database of purified proteins and known contaminants (*68*–*70*). MSFragger was used, and the precursor mass tolerance error was set to −20 to 20 parts per million (ppm). The fragment mass tolerance was set at 20 ppm. Protein digestion was set as nonspecific, searching between lengths of 4 and 50 amino acids, with a mass range of 400 to 5000 Da.

Mass analysis of peptide centroids and measurement of deuterium incorporation

HD-Examiner Software (Sierra Analytics) was used to automatically calculate the level of deuterium incorporation into each peptide. All peptides were manually inspected for correct charge state, correct retention time, appropriate selection of isotopic distribution, etc.

Absolute deuteration levels were calculated using the centroid of the experimental isotope clusters normalized to the fully deuterated control. Samples were only compared within a single experiment and were never compared to experiments completed at a different time with a different final D_2O level. The data analysis statistics for all HDX-MS experiments are in table S1 according to published guidelines (*71*). The mass spectrometry proteomics data have been deposited to the ProteomeXchange Consortium via the PRIDE partner repository (*72*) with the dataset identifier (PXD057548).

Immunoprecipitation

The DDD complex containing full-length DDB1, DET1, and DDA1 was produced in TNi cells. The complex was immobilized on Strep-TactinXT 4Flow resin (IBA Lifesciences) and analyzed for purity by SDS–polyacrylamide gel electrophoresis (PAGE) before immunoprecipitation.

A series of ubiquitin-conjugating enzymes (E2) were expressed in *E. coli* BL21 (DE3) cells. All constructs contained a His_6 affinity tag, either N-terminal (Ubc13, Ube2W, and Ube2e) or C-terminal [UbeE2K, Ube2T (1 to 153), Ube2T_FL, and UbcH5b]. Cells were lysed by sonication, and the proteins were purified by Ni^{2+} affinity chromatography as described above.

The His_6-E2 proteins were incubated with either the full-length DDD complex resin or Strep-TactinXT 4Flow resin, which was unbound at 4°C for 20 min with 50 mM tris-HCl (pH 8.0), 150 mM NaCl with 0.02% (v/v) Tween 20, and 2 mM DTT. After incubation, the resins were washed four times in this buffer. Samples were then resuspended in SDS sample buffer and visualized on 10 to 20% gradient SDS-PAGE stained with Coomassie R250.

Ubiquitination assays

Multiturnover assays

Multiturnover activity assays were carried out at 37°C for the indicated times to determine E3 activity of COP1. Reactions were carried out in a buffer containing 50 mM tris-HCl (pH 7.5), 50 mM NaCl, 2 mM $MgCl_2$, 2 mM TCEP (pH 7.0), and 5 mM ATP (pH 7.0).

Assays contained 0.1 μM E1, 10 μM E2 (either UbcH5b or Ube2e2), 50 μM Cy3-labeled ubiquitin, and 1 μM fluorescently labeled substrate (labeled with Alexa Fluor 647; AF647). If both UbcH5b and Ube2e2 were used, both were 10 μM. COP1, Cul4/Rbx1, and/or DDD were used at 3 μM, and the effect of these on substrate ubiquitination was assessed.

Samples were incubated at 37°C for the indicated time points, and the reaction was stopped by the addition of 4 × SDS-PAGE sample buffer. Fluorescently labeled proteins were detected using the Odyssey Fc imaging system (600 and/or 700 nM) prior to staining the gel with Coomassie R250.

Ubiquitin discharge assays

Ube2e2 was charged in a buffer containing 50 mM tris-HCl (pH 7.5), 50 mM NaCl, 2 mM $MgCl_2$, 2 mM TCEP (pH 7.0), and 5 mM ATP (pH 7.0). Reactions containing 1 μM E1, 60 μM dN-Ube2e2, and 150 μM ubiquitin were incubated at 37°C for 5 min. Following charging, the reaction was loaded onto a Superdex75 Increase 5/150 column (GE Life Sciences) and separated using a buffer containing 50 mM tris-HCl (pH 8.0) and 150 mM NaCl. The fractions containing charged Ube2e2 were collected and used in discharge assays.

Discharge assays were performed at 37°C for the indicated times to determine whether the DDD complex has any ability to cause ubiquitin discharge from charged E2 (Ube2e2). Reactions were performed in a buffer containing 50 mM tris-HCl (pH 8.0) and 150 mM NaCl. Assays contained the Ube2e2-Ub conjugate and 1 μM purified DDD (ΔBPB) complex. The positive and negative controls for these assays either replaced the DDD (ΔBPB) complex with RNF12 or omitted the DDD (ΔBPB) complex, respectively. Reactions were quenched with nonreducing SDS sample buffer and analyzed with SDS-PAGE stained with Coomassie R250.

Cell culture expression and downstream analysis

Expi293F were grown in Expi293 Expression Medium (Gibco, A1435102) supplemented with 1% penicillin-streptomycin (100 U/ml; Life Technologies, 15140122). Cells were grown at 37°C in a humidified atmosphere with 8% CO_2, shaking at 120 rpm. Expi293F cells were transiently transfected with Expifectamine 293 (Gibco, A14524). Cells were grown for 72 hours before being harvested by centrifugation at 800*g* for 10 min at 4°C. The cell pellet was washed with cold phosphate buffered saline and then either lysed with radioimmunoprecipitation assay (RIPA) (coexpression) or snap frozen (for copurifications).

Cells lysed with RIPA were incubated with RIPA buffer for 30 min on ice. The lysate was clarified by centrifugation at 10,000*g* and 4°C for 10 min, and the supernatant was snap frozen in liquid nitrogen to be used for subsequent analysis. All protein lysates were quantified using a bicinchoninic acid assay (Pierce BCA Protein Assay) and analyzed by Western blotting.

Copurification of DET1 by COP1

A series of mutations in both COP1 and DET1 were generated. COP1 (wild-type, loop mutants, or point mutations) and DET1 [full-length, cup deletion mutant (Δ), or point mutants] were expressed separately in Expi293F cells using Expifecatmine. The pellets of these were mixed before lysis and affinity purification of the StrepII-COP1. Clarified lysates were incubated with Strep-TactinXT 4Flow resin for 20 min at 4°C in rotation. The resin was washed four times in wash buffer supplemented with 0.02% (v/v) Tween 20, then resuspended in 4 × SDS-PAGE sample buffer, and then Western

blotted to determine whether DET1 could be retained by COP1. Lysates containing only DET1 were bound to Strep-TactinXT 4Flow resin to access nonspecific binding of DET1 to the resin itself.

Western blotting

For analysis by Western blot, samples were separated by SDS-PAGE and transferred to 0.2 μm of nitrocellulose (Life Technologies, IB23002). Membranes were blocked in 5% bovine serum albumin (BSA) (w/v) in Tris-buffered saline with Tween 20 buffer (TBS-T). Membranes were incubated with primary antibodies overnight at 4°C in 1 to 5% BSA (w/v) in TBS-T. Antibodies used were as follows: rabbit α-HA (1:5000, CST 3724), mouse α-COP1 (1:1000, Santa Cruz, C-terminal epitope, sc166799), rabbit-α-GST (1:1000, CST 2625), and/or mouse anti–α-tubulin (clone DM1A) (1:10,000, Millipore).

Following three washes with TBS-T, membranes were incubated with secondary antibodies diluted in TBS-T with 1% (w/v) BSA for 1 hour at room temperature. Secondary antibodies used were goat anti-rabbit IRdye 680LT (LI-COR) or goat anti-mouse IRdye 800LT (LI-COR). Membranes were washed a further three times with TBS-T. Membranes were then developed with the Odyssey Fc imaging system.

Supplementary Materials

The PDF file includes:

Figs. S1 to S7
Table S1
Legend for data S1

Other Supplementary Material for this manuscript includes the following:

Data S1

REFERENCES AND NOTES

1. C. Padovani, P. Jevtić, M. Rapé, Quality control of protein complex composition. *Mol. Cell* **82**, 1439–1450 (2022).
2. K. N. Swatek, D. Komander, Ubiquitin modifications. *Cell Res.* **26**, 399–422 (2016).
3. A. Scrima, R. Koníčková, B. K. Czyzewski, Y. Kawasaki, P. D. Jeffrey, R. Groisman, Y. Nakatani, S. Iwai, N. P. Pavletich, N. H. Thomä, Structural basis of UV DNA-damage recognition by the DDB1-DDB2 complex. *Cell* **135**, 1213–1223 (2008).
4. W. I. Mohamed, A. D. Schenk, G. Kempf, S. Cavadini, A. Basters, A. Potenza, W. Abdul Rahman, J. Rabl, K. Reichermeier, N. H. Thomä, The $CRL4^{DCAF1}$ cullin-RING ubiquitin ligase is activated following a switch in oligomerization state. *EMBO J.* **40**, e108008 (2021).
5. S. Fonseca, V. Rubio, Arabidopsis CRL4 complexes: Surveying chromatin states and gene expression. *Front. Plant Sci.* **10**, 1095 (2019).
6. M. D. Petroski, R. J. Deshaies, Function and regulation of cullin-RING ubiquitin ligases. *Nat. Rev. Mol. Cell Biol.* **6**, 9–20 (2004).
7. T. Li, E. I. Robert, P. C. van Breugel, M. Strubin, N. Zheng, A promiscuous α-helical motif anchors viral hijackers and substrate receptors to the CUL4-DDB1 ubiquitin ligase machinery. *Nat. Struct. Mol. Biol.* **17**, 105–111 (2010).
8. K. Baek, D. C. Scott, B. A. Schulman, NEDD8 and ubiquitin ligation by cullin-RING E3 ligases. *Curr. Opin. Struct. Biol.* **67**, 101–109 (2021).
9. N. Wei, X.-W. Deng, The COP9 signalosome. *Annu. Rev. Cell Dev. Biol.* **19**, 261–286 (2003).
10. S. Cavadini, E. S. Fischer, R. D. Bunker, A. Potenza, G. M. Lingaraju, K. N. Goldie, W. I. Mohamed, M. Faty, G. Petzold, R. E. J. Beckwith, R. B. Tichkule, U. Hassiepen, W. Abdulrahman, R. S. Pantelic, S. Matsumoto, K. Sugasawa, H. Stahlberg, N. H. Thomä, Cullin-RING ubiquitin E3 ligase regulation by the COP9 signalosome. *Nature* **531**, 598–603 (2016).
11. M. Békés, D. R. Langley, C. M. Crews, PROTAC targeted protein degraders: The past is prologue. *Nat. Rev. Drug Discov.* **21**, 181–200 (2022).
12. M. Nixdorf, U. Hoecker, SPA1 and DET1 act together to control photomorphogenesis throughout plant development. *Planta* **231**, 825–833 (2010).
13. O. S. Lau, X.-W. Deng, The photomorphogenic repressors COP1 and DET1: 20 years later. *Trends Plant Sci.* **17**, 584–593 (2012).
14. I. E. Wertz, K. M. O'Rourke, Z. Zhang, D. Dornan, D. Arnott, R. J. Deshaies, V. M. Dixit, Human De-etiolated-1 regulates c-Jun by assembling a CUL4A ubiquitin ligase. *Science* **303**, 1371–1374 (2004).
15. L. Rizzini, D. C. Levine, M. Perelis, J. Bass, C. B. Peek, M. Pagano, Cryptochromes-mediated inhibition of the CRL4Cop1-complex assembly defines an evolutionary conserved signaling mechanism. *Curr. Biol.* **29**, 1954–1962.e4 (2019).
16. E. Pick, O. S. Lau, T. Tsuge, S. Menon, Y. Tong, N. Dohmae, S. M. Plafker, X.-W. Deng, N. Wei, Mammalian DET1 regulates Cul4A activity and forms stable complexes with E2 ubiquitin-conjugating enzymes. *Mol. Cell. Biol.* **27**, 4708–4719 (2007).
17. K. Newton, D. L. Dugger, A. Sengupta-Ghosh, R. E. Ferrando, F. Chu, J. Tao, W. Lam, S. Haller, S. Chan, S. Sa, D. Dunlap, J. Eastham-Anderson, H. Ngu, J. Hung, D. M. French, J. D. Webster, B. Bolon, J. Liu, R. Reja, S. Kummerfeld, Y.-J. Chen, Z. Modrusan, J. W. Lewcock, V. M. Dixit, Ubiquitin ligase COP1 coordinates transcriptional programs that control cell type specification in the developing mouse brain. *Proc. Natl. Acad. Sci. U.S.A.* **115**, 11244–11249 (2018).
18. A. C. Vitari, K. G. Leong, K. Newton, C. Yee, K. O'Rourke, J. Liu, L. Phu, R. Vij, R. Ferrando, S. S. Couto, S. Mohan, A. Pandita, J.-A. Hongo, D. Arnott, I. E. Wertz, W.-Q. Gao, D. M. French, V. M. Dixit, COP1 is a tumour suppressor that causes degradation of ETS transcription factors. *Nature* **474**, 403–406 (2011).
19. P. H. Dedhia, K. Keeshan, S. Uljon, L. Xu, M. E. Vega, O. Shestova, M. Zaks-Zilberman, C. Romany, S. C. Blacklow, W. S. Pear, Differential ability of Tribbles family members to promote degradation of C/EBPα and induce acute myelogenous leukemia. *Blood* **116**, 1321–1328 (2010).
20. S. A. Jamieson, Z. Ruan, A. E. Burgess, J. R. Curry, H. D. McMillan, J. L. Brewster, A. K. Dunbier, A. D. Axtman, N. Kannan, P. D. Mace, Substrate binding allosterically relieves autoinhibition of the pseudokinase TRIB1. *Sci. Signal.* **11**, eaau0597 (2018).
21. Z. Zhang, K. Newton, S. K. Kummerfeld, J. Webster, D. S. Kirkpatrick, L. Phu, J. Eastham-Anderson, J. Liu, W. P. Lee, J. Wu, H. Li, M. R. Junttila, V. M. Dixit, Transcription factor Etv5 is essential for the maintenance of alveolar type II cells. *Proc. Natl. Acad. Sci. U.S.A.* **114**, 3903–3908 (2017).
22. R. C. Bauer, M. Sasaki, D. M. Cohen, J. Cui, M. A. Smith, B. O. Yenilmez, D. J. Steger, D. J. Rader, Tribbles-1 regulates hepatic lipogenesis through posttranscriptional regulation of C/EBPα. *J. Clin. Invest.* **125**, 3809–3818 (2015).
23. R. Suriben, K. A. Kaihara, M. Paolino, M. Reichelt, S. K. Kummerfeld, Z. Modrusan, D. L. Dugger, K. Newton, M. Sagolla, J. D. Webster, J. Liu, M. Hebrok, V. M. Dixit, β-cell insulin secretion requires the ubiquitin ligase COP1. *Cell* **163**, 1457–1467 (2015).
24. X. Wang, C. Tokheim, S. S. Gu, B. Wang, Q. Tang, Y. Li, N. Traugh, Z. Zeng, Y. Zhang, Z. Li, B. Zhang, J. Fu, T. Xiao, W. Li, C. A. Meyer, J. Chu, P. Jiang, P. Cejas, K. Lim, H. Long, M. Brown, X. S. Liu, In vivo CRISPR screens identify the E3 ligase Cop1 as a modulator of macrophage infiltration and cancer immunotherapy target. *Cell* **184**, 5357–5374.e22 (2021).
25. J.-C. Marine, Spotlight on the role of COP1 in tumorigenesis. *Nat. Rev. Cancer* **12**, 455–464 (2012).
26. A. Ndoja, R. Reja, S.-H. Lee, J. D. Webster, H. Ngu, C. M. Rose, D. S. Kirkpatrick, Z. Modrusan, Y.-J. J. Chen, D. L. Dugger, V. Gandham, L. Xie, K. Newton, V. M. Dixit, Ubiquitin ligase COP1 suppresses neuroinflammation by degrading c/EBPβ in microglia. *Cell* **182**, 1156–1169.e12 (2020).
27. Y. Xie, Z. Cao, E. W. Wong, Y. Guan, W. Ma, J. Q. Zhang, E. G. Walczak, D. Murphy, L. Ran, I. Sirota, S. Wang, S. Shukla, D. Gao, S. R. Knott, K. Chang, J. Leu, J. Wongvipat, C. R. Antonescu, G. Hannon, P. Chi, Y. Chen, COP1/DET1/ETS axis regulates ERK transcriptome and sensitivity to MAPK inhibitors. *J. Clin. Invest.* **128**, 1442–1457 (2018).
28. S. Angers, T. Li, X. Yi, M. J. MacCoss, R. T. Moon, N. Zheng, Molecular architecture and assembly of the DDB1-CUL4A ubiquitin ligase machinery. *Nature* **443**, 590–593 (2006).
29. E. R. Watson, S. Novick, M. E. Matyskiela, P. P. Chamberlain, A. H. de la Peña, J. Zhu, E. Tran, P. R. Griffin, I. E. Wertz, G. C. Lander, Molecular glue CELMoD compounds are regulators of cereblon conformation. *Science* **378**, 549–553 (2022).
30. D. E. Bussiere, L. Xie, H. Srinivas, W. Shu, A. Burke, C. Be, J. Zhao, A. Godbole, D. King, R. G. Karki, V. Hornak, F. Xu, J. Cobb, N. Carte, A. O. Frank, A. Frommlet, P. Graff, M. Knapp, A. Fazal, B. Okram, S. Jiang, P.-Y. Michellys, R. Beckwith, H. Voshol, C. Wiesmann, J. M. Solomon, J. Paulk, Structural basis of indisulam-mediated RBM39 recruitment to DCAF15 E3 ligase complex. *Nat. Chem. Biol.* **16**, 15–23 (2020).
31. X. Du, O. A. Volkov, R. M. Czerwinski, H. Tan, C. Huerta, E. R. Morton, J. P. Rizzi, P. M. Wehn, R. Xu, D. Nijhawan, E. M. Wallace, Structural basis and kinetic pathway of RBM39 recruitment to DCAF15 by a sulfonamide molecular glue E7820. *Structure* **27**, 1625–1633.e3 (2019).
32. G. R. Masson, M. L. Jenkins, J. E. Burke, An overview of hydrogen deuterium exchange mass spectrometry (HDX-MS) in drug discovery. *Expert Opin. Drug Discov.* **12**, 981–994 (2017).
33. D. Goswami, S. Devarakonda, M. J. Chalmers, B. D. Pascal, B. M. Spiegelman, P. R. Griffin, Time window expansion for HDX analysis of an intrinsically disordered protein. *J. Am. Soc. Mass Spectrom.* **24**, 1584–1592 (2013).

34. Y. Bai, J. S. Milne, L. Mayne, S. W. Englander, Primary structure effects on peptide group hydrogen exchange. *Proteins* **17**, 75–86 (1993).
35. J. Jumper, R. Evans, A. Pritzel, T. Green, M. Figurnov, O. Ronneberger, K. Tunyasuvunakool, R. Bates, A. Žídek, A. Potapenko, A. Bridgland, C. Meyer, S. A. A. Kohl, A. J. Ballard, A. Cowie, B. Romera-Paredes, S. Nikolov, R. Jain, J. Adler, T. Back, S. Petersen, D. Reiman, E. Clancy, M. Zielinski, M. Steinegger, M. Pacholska, T. Berghammer, S. Bodenstein, D. Silver, O. Vinyals, A. W. Senior, K. Kavukcuoglu, P. Kohli, D. Hassabis, Highly accurate protein structure prediction with AlphaFold. *Nature* **596**, 583–589 (2021).
36. P. S. Brzovic, A. Lissounov, D. E. Christensen, D. W. Hoyt, R. E. Klevit, A UbcH5/ubiquitin noncovalent complex is required for processive BRCA1-directed ubiquitination. *Mol. Cell* **21**, 873–880 (2006).
37. L. Buetow, M. Gabrielsen, N. G. Anthony, H. Dou, A. Patel, H. Aitkenhead, G. J. Sibbet, B. O. Smith, D. T. Huang, Activation of a primed RING E3-E2-ubiquitin complex by non-covalent ubiquitin. *Mol. Cell* **58**, 297–310 (2015).
38. M. D. Stewart, T. Ritterhoff, R. E. Klevit, P. S. Brzovic, E2 enzymes: More than just middle men. *Cell Res.* **26**, 423–440 (2016).
39. A. J. Middleton, J. Zhu, C. L. Day, The RING domain of RING finger 12 efficiently builds degradative ubiquitin chains. *J. Mol. Biol.* **432**, 3790–3801 (2020).
40. U. Hoecker, The activities of the E3 ubiquitin ligase COP1/SPA, a key repressor in light signaling. *Curr. Opin. Plant Biol.* **37**, 63–69 (2017).
41. K. Baek, D. T. Krist, J. R. Prabu, S. Hill, M. Klügel, L.-M. Neumaier, S. von Gronau, G. Kleiger, B. A. Schulman, NEDD8 nucleates a multivalent cullin-RING-UBE2D ubiquitin ligation assembly. *Nature* **578**, 461–466 (2020).
42. J. Abramson, J. Adler, J. Dunger, R. Evans, T. Green, A. Pritzel, O. Ronneberger, L. Willmore, A. J. Ballard, J. Bambrick, S. W. Bodenstein, D. A. Evans, C.-C. Hung, M. O'Neill, D. Reiman, K. Tunyasuvunakool, Z. Wu, A. Žemgulytė, E. Arvaniti, C. Beattie, O. Bertolli, A. Bridgland, A. Cherepanov, M. Congreve, A. I. Cowen-Rivers, A. Cowie, M. Figurnov, F. B. Fuchs, H. Gladman, R. Jain, Y. A. Khan, C. M. R. Low, K. Perlin, A. Potapenko, P. Savy, S. Singh, A. Stecula, A. Thillaisundaram, C. Tong, S. Yakneen, E. D. Zhong, M. Zielinski, A. Žídek, V. Bapst, P. Kohli, M. Jaderberg, D. Hassabis, J. M. Jumper, Accurate structure prediction of biomolecular interactions with AlphaFold 3. *Nature* **630**, 493–500 (2024).
43. Y. Sunami, S. Yoshino, Y. Yamazaki, T. Iwamoto, T. Nakamura, Rapid increase of C/EBPα p42 induces growth arrest of acute myeloid leukemia (AML) cells by Cop1 deletion in Trib1-expressing AML. *Leukemia* **38**, 2585–2597 (2024).
44. P. V. Hornbeck, B. Zhang, B. Murray, J. M. Kornhauser, V. Latham, E. Skrzypek, PhosphoSitePlus, 2014: Mutations, PTMs and recalibrations. *Nucleic Acids Res.* **43**, D512–D520 (2014).
45. D. E. Christensen, P. S. Brzovic, R. E. Klevit, E2-BRCA1 RING interactions dictate synthesis of mono- or specific polyubiquitin chain linkages. *Nat. Struct. Mol. Biol.* **14**, 941–948 (2007).
46. P. A. Banka, A. P. Behera, S. Sarkar, A. B. Datta, RING E3-catalyzed E2 self-ubiquitination attenuates the activity of Ube2E ubiquitin-conjugating enzymes. *J. Mol. Biol.* **427**, 2290–2304 (2015).
47. L. Nguyen, K. S. Plafker, A. Starnes, M. Cook, R. E. Klevit, S. M. Plafker, The ubiquitin-conjugating enzyme, UbcM2, is restricted to monoubiquitylation by a two-fold mechanism that involves backside residues of E2 and Lys48 of ubiquitin. *Biochemistry* **53**, 4004–4014 (2014).
48. F.-R. Schumacher, G. Wilson, C. L. Day, The N-terminal extension of UBE2E ubiquitin-conjugating enzymes limits chain assembly. *J. Mol. Biol.* **425**, 4099–4111 (2013).
49. G. Suzuki, Y. Yanagawa, S. F. Kwok, M. Matsui, X.-W. Deng, Arabidopsis COP10 is a ubiquitin-conjugating enzyme variant that acts together with COP1 and the COP9 signalosome in repressing photomorphogenesis. *Genes Dev.* **16**, 554–559 (2002).
50. Y. Yanagawa, J. A. Sullivan, S. Komatsu, G. Gusmaroli, G. Suzuki, J. Yin, T. Ishibashi, Y. Saijo, V. Rubio, S. Kimura, J. Wang, X. W. Deng, Arabidopsis COP10 forms a complex with DDB1 and DET1 in vivo and enhances the activity of ubiquitin conjugating enzymes. *Genes Dev.* **18**, 2172–2181 (2004).
51. D. Horn-Ghetko, D. T. Krist, J. R. Prabu, K. Baek, M. P. C. Mulder, M. Klügel, D. C. Scott, H. Ovaa, G. Kleiger, B. A. Schulman, Ubiquitin ligation to F-box protein targets by SCF-RBR E3-E3 super-assembly. *Nature* **590**, 671–676 (2021).
52. J. Li, N. Purser, J. Liwocha, D. C. Scott, H. A. Byers, B. Steigenberger, S. Hill, I. Tripathi-Giesgen, T. Hinkle, F. M. Hansen, J. R. Prabu, S. K. Radhakrishnan, D. S. Kirkpatrick, K. M. Reichermeier, B. A. Schulman, G. Kleiger, Cullin-RING ligases employ geometrically optimized catalytic partners for substrate targeting. *Mol. Cell* **84**, 1304–1320.e16 (2024).
53. Y.-D. Li, M. W. Ma, M. M. Hassan, M. Hunkeler, M. Teng, K. Puvar, R. Lumpkin, B. Sandoval, C. Y. Jin, S. B. Ficarro, M. Y. Wang, S. Xu, B. J. Groendyke, L. H. Sigua, I. Tavares, C. Zou, J. M. Tsai, P. M. C. Park, H. Yoon, F. C. Majewski, J. A. Marto, J. Qi, R. P. Nowak, K. A. Donovan, M. Słabicki, N. S. Gray, E. S. Fischer, B. L. Ebert, Template-assisted covalent modification of DCAF16 underlies activity of BRD4 molecular glue degraders. *Nat. Chem. Biol.* **20**, 1640–1649 (2024).
54. O. Hsia, M. Hinterndorfer, A. D. Cowan, K. Iso, T. Ishida, R. Sundaramoorthy, M. A. Nakasone, H. Imrichova, C. Schätz, A. Rukavina, K. Husnjak, M. Wegner, A. Correa-Sáez, C. Craigon, R. Casement, C. Maniaci, A. Testa, M. Kaulich, I. Dikic, G. E. Winter, A. Ciulli, Targeted protein degradation via intramolecular bivalent glues. *Nature* **627**, 204–211 (2024).
55. P. A. Eyers, K. Keeshan, N. Kannan, Tribbles in the 21st century: The evolving roles of tribbles pseudokinases in biology and disease. *Trends Cell Biol.* **27**, 284–298 (2017).
56. S. A. Jamieson, M. Pudjihartono, C. R. Horne, J. S. Viloria, J. L. Dunlop, H. D. McMillan, R. C. Day, K. Keeshan, J. M. Murphy, P. D. Mace, Nanobodies identify an activated state of the TRIB2 pseudokinase. *Structure* **30**, 1518–1529.e5 (2022).
57. S. Uljon, X. Xu, I. Durzynska, S. Stein, G. Adelmant, J. A. Marto, W. S. Pear, S. C. Blacklow, Structural basis for substrate selectivity of the E3 ligase COP1. *Structure* **24**, 687–696 (2016).
58. K. M. Reichermeier, R. Straube, J. M. Reitsma, M. J. Sweredoski, C. M. Rose, A. Moradian, W. den Besten, T. Hinkle, E. Verschueren, G. Petzold, N. H. Thomä, I. E. Wertz, R. J. Deshaies, D. S. Kirkpatrick, PIKES analysis reveals response to degraders and key regulatory mechanisms of the CRL4 network. *Mol. Cell* **77**, 1092–1106.e9 (2020).
59. F. Weissmann, G. Petzold, R. VanderLinden, P. J. Huis in 't Veld, N. G. Brown, F. Lampert, S. Westermann, H. Stark, B. A. Schulman, J.-M. Peters, biGBac enables rapid gene assembly for the expression of large multisubunit protein complexes. *Proc. Natl. Acad. Sci. U.S.A.* **113**, E2564–E2569 (2016).
60. A. Paluda, A. J. Middleton, C. Rossig, P. D. Mace, C. L. Day, Ubiquitin and a charged loop regulate the ubiquitin E3 ligase activity of Ark2C. *Nat. Commun.* **13**, 1181 (2022); https://doi.org/10.1038/s41467-022-28782-y.
61. A. Punjani, J. L. Rubinstein, D. J. Fleet, M. A. Brubaker, cryoSPARC: algorithms for rapid unsupervised cryo-EM structure determination. *Nat. Methods* **14**, 290–296 (2017); https://doi.org/10.1038/nmeth.4169.
62. J. Zivanov, T. Nakane, B. O. Forsberg, D. Kimanius, W. J. Hagen, E. Lindahl, S. H. Scheres, New tools for automated high-resolution cryo-EM structure determination in RELION-3. *eLife* **7**, e42166 (2018); https://doi.org/10.7554/elife.42166.
63. R. Sanchez-Garcia, J. Gomez-Blanco, A. Cuervo, J. M. Carazo, C. O. S. Sorzano, J. Vargas, DeepEMhancer: a deep learning solution for cryo-EM volume post-processing. *Commun Biol*. **4**, 874 (2021); https://doi.org/10.1038/s42003-021-02399-1.
64. Y. Z. Tan, P. R. Baldwin, J. H. Davis, J. R. Williamson, C. S. Potter, B. Carragher, D. Lyumkis, Addressing preferred specimen orientation in single-particle cryo-EM through tilting. *Nat. Methods* **14**, 793–796 (2017); https://doi.org/10.1038/nmeth.4347.
65. A. Morin, B. Eisenbraun, J. Key, P. C. Sanschagrin, M. A. Timony, M. Ottaviano, P. Sliz, Collaboration gets the most out of software. *eLife* **2**, e01456 (2013); https://doi.org/10.7554/elife.01456.
66. P. Bryant, F. Noé, Improved protein complex prediction with AlphaFold-multimer by denoising the MSA profile. bioRxiv 2023.07.04.547638 [Preprint] (2023). https://doi.org/10.1101/2023.07.04.547638.
67. J. T. B. Stariha, R. M. Hoffmann, D. J. Hamelin, J. E. Burke, Probing protein-membrane interactions and dynamics using hydrogen-deuterium exchange mass spectrometry (HDX-MS). *Methods Mol. Biol.* **2263**, 465–485 (2021).
68. A. T. Kong, F. V. Leprevost, D. M. Avtonomov, D. Mellacheruvu, A. I. Nesvizhskii, MSFragger: Ultrafast and comprehensive peptide identification in mass spectrometry-based proteomics. *Nat. Methods* **14**, 513–520 (2017).
69. J. M. Dobbs, M. L. Jenkins, J. E. Burke, *Escherichia coli* and Sf9 contaminant databases to increase efficiency of tandem mass spectrometry peptide identification in structural mass spectrometry experiments. *J. Am. Soc. Mass Spectrom.* **31**, 2202–2209 (2020).
70. F. da Veiga Leprevost, S. E. Haynes, D. M. Avtonomov, H.-Y. Chang, A. K. Shanmugam, D. Mellacheruvu, A. T. Kong, A. I. Nesvizhskii, Philosopher: A versatile toolkit for shotgun proteomics data analysis. *Nat. Methods* **17**, 869–870 (2020).
71. G. R. Masson, J. E. Burke, N. G. Ahn, G. S. Anand, C. Borchers, S. Brier, G. M. Bou-Assaf, J. R. Engen, S. W. Englander, J. Faber, R. Garlish, P. R. Griffin, M. L. Gross, M. Guttman, Y. Hamuro, A. J. R. Heck, D. Houde, R. E. Iacob, T. J. D. Jørgensen, I. A. Kaltashov, J. P. Klinman, L. Konermann, P. Man, L. Mayne, B. D. Pascal, D. Reichmann, M. Skehel, J. Snijder, T. S. Strutzenberg, E. S. Underbakke, C. Wagner, T. E. Wales, B. T. Walters, D. D. Weis, D. J. Wilson, P. L. Wintrode, Z. Zhang, J. Zheng, D. C. Schriemer, K. D. Rand, Recommendations for performing, interpreting and reporting hydrogen deuterium exchange mass spectrometry (HDX-MS) experiments. *Nat. Methods* **16**, 595–602 (2019).
72. Y. Perez-Riverol, J. Bai, C. Bandla, D. García-Seisdedos, S. Hewapathirana, S. Kamatchinathan, D. J. Kundu, A. Prakash, A. Frericks-Zipper, M. Eisenacher, M. Walzer, S. Wang, A. Brazma, J. A. Vizcaíno, The PRIDE database resources in 2022: A hub for mass spectrometry-based proteomics evidences. *Nucleic Acids Res.* **50**, D543–D552 (2022).

Acknowledgments: We thank and acknowledge the use of the University of Wollongong Cryogenic Electron Microscopy Facility at Molecular Horizons. Special thanks to the Day Lab (University of Otago) for their collaboration and for generously sharing various DNA constructs and ubiquitin-related reagents. We thank SBGrid for compilation of structural biology software, and also thank P. Higbee (Research IT, Otago) for expertise assistance, which contributed to the success of our project. We express our appreciation to the Electron Microscopy (EM) facility at Otago for technical assistance. **Funding:** This work was supported by the Marsden Fund Grant UOO2102 (P.D.M.), Royal Society of New Zealand Catalyst Seeding

Grant 21-UOO-003-CSG (P.D.M.), Otago University Postgraduate PhD Scholarship (T.A.L. and J.L.D.), Otago University Division of Health Sciences Postdoctoral Career Development Fellowship (L.S.T.), Otago University Marjorie McCallum Travel Award (T.A.L.), SNSF Swiss Postdoctoral Fellowship Grant 210216 (P.F.), and Natural Science and Engineering Research Council (Discovery Grant NSERC-2020-04241; J.E.B.). **Author contributions:** Conceptualization: P.D.M., A.E.B., and T.A.L. Methodology: P.D.M., A.E.B., T.A.L., S.H.J.B., S.A.J., H.G.N., and J.E.B. Investigation: P.D.M., A.E.B., T.A.L., S.H.J.B., S.A.J., P.F., J.R.C., L.S.T., J.L.D., and H.G.N. Visualization: P.D.M., A.E.B., T.A.L., P.F., and H.G.N. Supervision: P.D.M. and J.E.B. Writing—original draft: P.D.M., A.E.B., T.A.L., and J.L.D. Writing—review and editing: P.D.M., A.E.B., T.A.L., H.G.N., S.H.J.B., J.E.B., S.A.J., P.F., L.S.T., and J.L.D. Funding acquisition: P.D.M. and S.H.J.B. **Competing interests:** P.D.M. serves in a general capacity as a scientific advisory board member for Arvinas Inc. The authors declare that they have no other competing interests. **Data and materials availability:** The mass spectrometry proteomics data have been deposited to the ProteomeXchange Consortium via the PRIDE partner repository (*72*) with the dataset identifier (PXD057548). The cryo-EM map and structure of the DDB1(ΔBPB)-DET1-DDA1-Ube2e2 complex has been deposited in the EMDB, with the deposition ID (EMD-44638) and the PDB with identifier 9bjz. All other data needed to evaluate the conclusions in the paper are present in the paper and/or the Supplementary Materials.

Submitted 17 May 2024
Accepted 24 January 2025
Published 26 February 2025
10.1126/sciadv.adq4187